GEOLOGICA CARPATHICA, APRIL 2021, 72, 2, 134–154 https://doi.org/10.31577/GeolCarp.72.2.4

Magnetic fabrics in the turbidite deposits of the Central Carpathian Paleogene Basin in relation to sedimentary and tectonic fabric elements

JOZEF MADZIN[1,✉], EMŐ MÁRTON[2], DUŠAN STAREK[3] and TOMÁŠ MIKUŠ[1]

[1]Earth Science Institute, Slovak Academy of Sciences, Ďumbierska 1, 974 01 Banská Bystrica, Slovakia; ✉jozef.madzin@savba.sk, mikus@savbb.sk
[2]Mining and Geological Survey of Hungary, Paleomagnetic Laboratory, Columbus 17-23, H-1145 Budapest, Hungary; paleo@mbfsz.gov.hu
[3]Earth Science Institute, Slovak Academy of Sciences, Dúbravská cesta 9, 840 05 Bratislava, Slovakia; dusan.starek@savba.sk

(Manuscript received December 8, 2020; accepted in revised form March 23, 2021; Associate Editor: Ján Soták)

Abstract: Anisotropy of magnetic susceptibility and anisotropy of anhysteretic remanent magnetization were studied in the Oligocene turbidites of the weakly deformed Central Carpathian Paleogene Basin. In order to decide whether the magnetic fabric can be related to deposition from a paleoflow or to incipient weak tectonic deformation we compared magnetic fabrics in individual intervals of the Bouma sequence with sedimentary structures and tectonic brittle mesostructures (joints). In the Ta–Te intervals we observed a good correlation between maximum susceptibility axes and SW(W)–NE(E) oriented paleoflows. Within convoluted and slump folded sandstones the AMS fabric coincides with the orientation of soft-sediment deformation structures. These features suggest the sedimentary origin of the AMS fabric. Three types of AARM sub-fabric were distinguished. The AARM type 1 represents magnetic foliations parallel either to NNW–SSE or to NE–SW oriented joints with magnetic lineations distributed along the joins. In the AARM type 2 magnetic foliations remained parallel to the bedding while magnetic lineations group around the joint to bedding intersections. The AARM type 3 coincides with the AMS fabric. Magnetic and microscopic analyses indicate that the AARM fabrics are connected to magnetite associated with subordinate ferrimagnetic iron sulphides. Both minerals occur in a sub-microscopic size and formed most likely during late diagenesis through the alteration of pyrite, possibly accompanied by burial clay transformation processes. The growth of the authigenic ferrimagnetic minerals was conditioned by combined effects of the sedimentary petrofabric, lithology and stress conditions during the inversion of the basin in the Early to Middle Miocene.

Keywords: turbidite facies, magnetic fabrics, sedimentary structures, paleoflows, joints, Central Carpathian Paleogene Basin.

Introduction

The study of magnetic fabric, including the measurements of the anisotropy of magnetic susceptibility (AMS), anisotropy of anhysteretic (AARM) or isothermal remanent magnetization (AIRM), has been a well-recognized petrofabric tool among geoscientists for decades (Hrouda 1982; Tarling & Hrouda 1993; Parés et al. 1999; Borradaile & Jackson 2010; Parés 2015 for review). The magnetic fabric has been used to reveal the preferred orientation in various types of rocks (e.g. Averbuch et al. 1992; Gregorová et al. 2009; Tomek et al. 2014; Závada et al. 2017) and was documented as an especially sensitive strain marker in low-deformation settings (e.g. Cifelli et al. 2009; Mattei et al. 1997; Soto et al. 2009).

In sedimentary rocks, the magnetic fabric may reflect the mutual arrangement and orientation of all dia-, para- and ferromagnetic s.l. particles attained during the transport and deposition, successfully used to detect flow directions (e.g. Rees 1965; Taira & Scholle 1979; Baas et al. 2007; Veloso et al. 2007; Dall'Olio et al. 2013; Felletti et al. 2016). However, the primary sedimentary magnetic fabric can be partly or completely reoriented by syn- and early post-depositional processes (Pueyo Anchuela et al. 2011; García-Lasanta et al. 2013), diagenesis (Larrasoaña et al. 2004) and/or tectonic deformation acting already during or after deposition in both extensional (Mattei et al. 1999; Cifelli et al. 2005) and compressional settings (Parés et al. 1999; Soto et al. 2009; Márton et al. 2012).

Water flow-generated magnetic fabrics in sedimentary rocks are characterized by oblate anisotropy ellipsoid lying parallel to the bedding plane with maximum susceptibility axes (Kmax; magnetic lineations) aligned parallel to the flow direction, often gently inclined up-current (Tarling & Hrouda 1993). In fast flowing currents (≥1cm/s) or on steep slopes Kmax may occasionally become oriented perpendicular or even oblique to the flow direction (Baas et al. 2007). In the case of incipient deformation the Kmax rotate to the position perpendicular to the compression, while minimum susceptibility axes (Kmin; pole to the magnetic foliation) remain near the bedding poles (Kissel et al. 1986; Parés et al. 1999; Hrouda et al. 2009). In extensional settings Kmax coincides with the maximum extension direction, which is usually parallel to the bedding dip (Mattei et al. 1999; Cifelli et al. 2005). Deposition from a water current and weak tectonic deformation can,

therefore, produce very similar magnetic fabrics, and thus it may be difficult to differentiate their origin (Dall'Olio et al. 2013).

In the Central Carpathian Paleogene Basin (CCPB) (Fig. 1), which represents a relatively weakly deformed fore-arc basin, a primary sedimentary or transitional sedimentary to weak tectonic deformation magnetic fabric in turbidite sandstones has been reported (Hrouda & Potfaj 1993; Hrouda et al. 2018). In previous magnetic fabric studies of fine-grained deposits of the CCPB a sedimentary magnetic fabric has been observed, inferring that the magnetic lineation could serve as a proxy for paleoflow directions (Márton et al. 1999; 2009a). In the Oligocene turbidites of the CCPB sedimentological methods indicate sedimentary transport mostly from W to E and from SW to NE in the Liptov, Orava and Podhale Basins (Fig. 1B,C) (Marschalko & Radomski 1960; Soták et al. 2001; Králiková et al. 2014; Starek & Fuksi 2017a,b; Starek et al. 2019). Opposite directions from E to W or from SE to NW and subordinate directions from NE to SW were measured in the Levočské vrchy Mts. and Šarišská vrchovina Upland (Fig. 1B,C) (Marschalko 1968, 1970; Marschalko & Gross 1970; Janočko et al. 1998; Soták et al. 2001; Janočko 2002).

Paleostress analyses of brittle and semibrittle structures in the CCPB showed the progressive clockwise rotation of the compressive paleostress field from NW–SE to NE–SW during the Miocene (Pešková et al. 2009; Vojtko et al. 2010; Sůkalová et al. 2012; Králiková et al. 2014). This must have

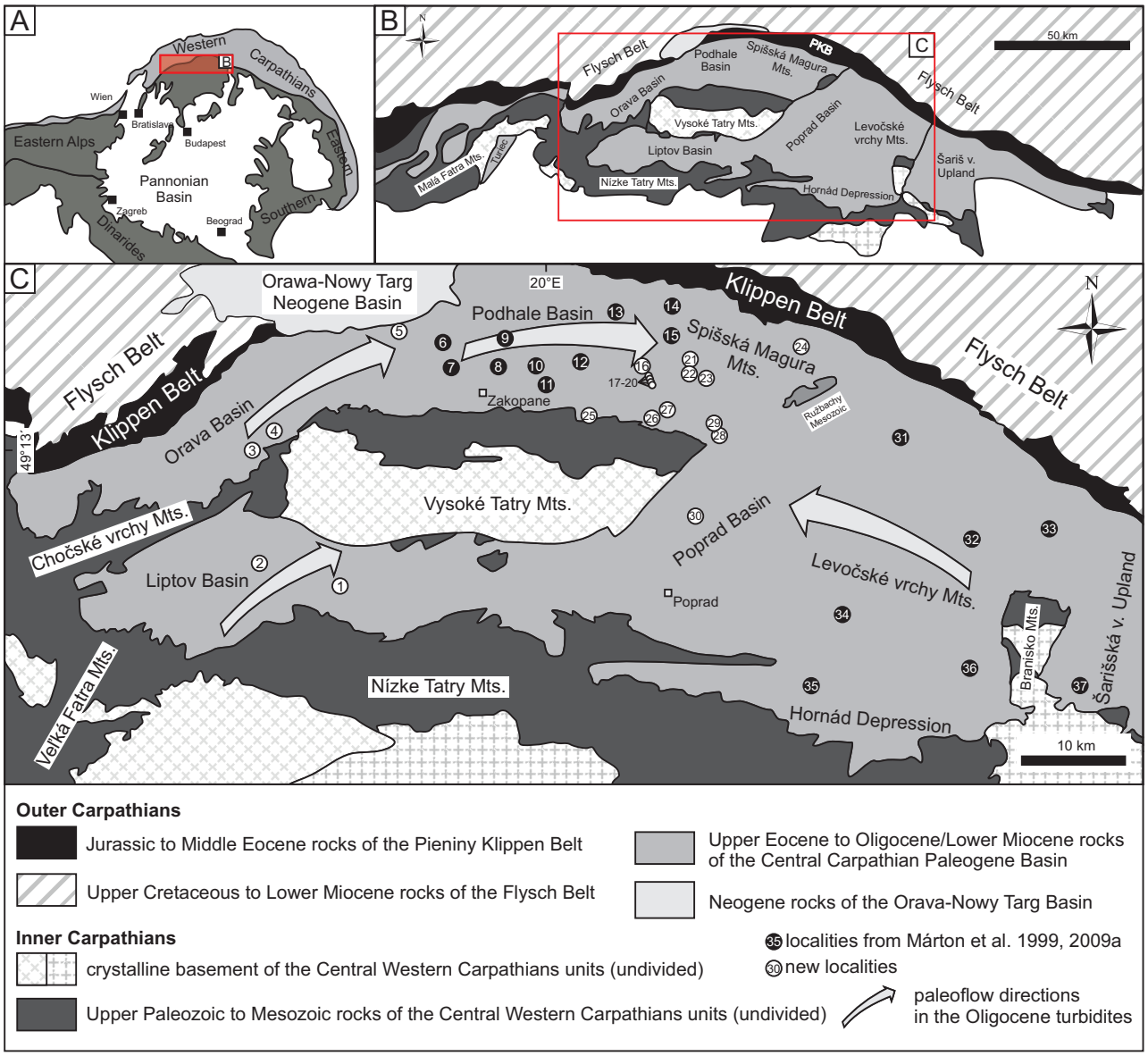

Fig. 1. A — Geological map showing the location of the studied area within the framework of the Alpine-Carpathian region; **B** — the CCPB system occupying several intramontane sub-basins surrounded by uplifted core mountains; **C** — geological sketch map of the study area (based on Bezák et al. 2004; Starek et al. 2012) with the sampling sites and general paleoflow directions in the Oligocene turbidites (see text for citations).

been an apparent paleostress field rotation as a result of the Miocene en-mass counterclockwise rotation of the Outer and Inner Western Carpathians in a stress field of roughly N–S oriented compression (Márton & Fodor 1995, 2003; Márton et al. 1999, 2009a,b, 2013, 2016; Márton 2020). In the general frame of sedimentary transport directions as well as of the stress field orientation, the magnetic fabrics in the weakly deformed rocks of the CCPB were interpreted either as oriented by turbidity currents (Márton et al. 1999, 2009a) or by the tectonic deformation (Hrouda & Potfaj 1993; Hrouda et al. 2018). In order to decide about the dominance of one or the other of the governing factors in orienting the magnetic fabrics, we studied several outcrops in turbidite deposits of the CCPB where direct comparison between magnetic fabrics (AMS, AARM) and orientation of sedimentary structures (bedding, flute casts, slump folds) and mesoscopic brittle structures (prevailingly joints) was possible. Comparison of magnetic fabrics between individual turbidite facies (Ta–Te intervals *sensu* Bouma 1962) and syn- or early post-sedimentary hydroplastically deformed facies seems to be an especially effective way to distinguish a primary sedimentary or tectonic deformation origin of magnetic fabrics (Piper et al. 1996; Dall'Olio et al. 2013; Felletti et al. 2016; Stachowska et al. 2020).

Geological settings

The CCPB formed within the Western Carpathians as a forearc basin system on the Alpine–Carpathian–Pannonian destructive margin behind the Outer Carpathian accretionary wedge (Royden & Baldi 1988; Tari et al. 1993; Soták et al. 2001; Kázmér et al. 2003; Kováč et al. 2016). It belongs to the basin system of Peri- and Para-Tethyan seas and represents the largest accommodation space of submarine fan deposits in the Central Western Carpathians (Soták et al. 2001).

The remnants of the basin have been preserved in several intramontane basins situated between uplifted basement-involved horst structures known as "core mountains" of the Central Western Carpathians (Plašienka et al. 1997; Plašienka 2018) (Fig. 1). The deposits of the CCPB overlie the Central Western Carpathian nappe units, which consolidated during the pre-Senonian thrusting (Plašienka 2018). The northern boundary is tectonic, represented by the Pieniny Klippen Belt, which is a complex transpressional strike-slip shear zone considered as a suture zone (Ratschbacher et al. 1993; Kováč & Hók 1996; Plašienka et al. 2019).

The sedimentary fill of the CCPB is composed mostly of turbidite-like sediments covering the time span from the Bartonian to the end of the Oligocene or up to the lowermost Miocene (Olszewska & Wieczorek 1998; Gedl 2000; Garecka 2005; Soták 2010; Starek et al. 2019). In Slovakia, the CCPB is formally divided into four formations of the Podtatranská skupina Group (Gross et al. 1984; Fig. 2). The lowermost Borové Fm. is represented by terrestrial deposits covered by carbonate platform sediments known as the "Numulitic Eocene"

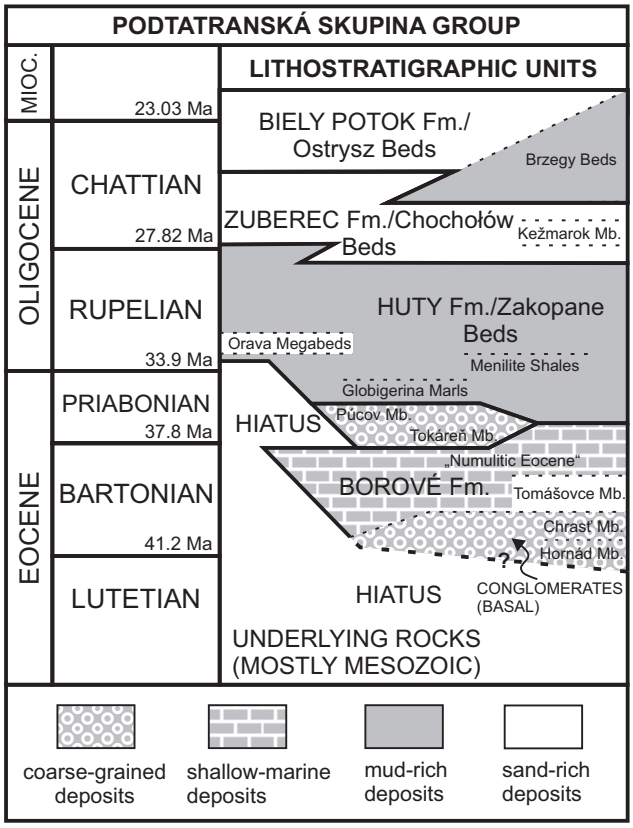

Fig. 2. Lithostratigraphic column of the Late Eocene to Oligocene/earliest Miocene sedimentary succession of the CCPB (based on Gross et al. 1984; Filo & Siráňová 1996, 1998; Olszewska & Wieczorek 1998; Starek et al. 2000, 2012; Soták et al. 2001, 2007; Gross 2008).

in Poland (Gołab 1959; Roniewicz 1969). The Borové Fm. also includes regressive–transgressive cycles of alluvial fan and fluvial deposits (Hornád Mb. and Chrasť Mb., Filo & Siráňová 1996). Shallow-marine fluvio-deltaic sediments of the Tomášovce Mb. (Filo & Siráňová 1998) are exposed mainly in the Levočské vrchy Mts. and in the Hornád Depression. The dynamic environment is recorded by the lateral input of coarse-grained deposits of the Pucov Mb. in the Orava region (Gross et al. 1982, 1984; Starek et al. 2012) and Tokáreň conglomerates in the Spišská Magura Mts. (Janočko & Jacko 1998; Janočko et al. 2000). These sediments deposited during important relative sea level changes at tectonically active basin margins in the Late Eocene (Starek et al. 2012). The Borové Fm. is overlain by the Huty Fm., a.k.a. the Zakopane Beds, which consists of mud-rich deposits with horizons of Globigerina Marls and dysoxic Menilite Shales (Soták et al. 2007; Soták 2010). Above the Menilite Shales unusually thick sandstone–siltstone–claystone turbidite beds appear. They are called the Orava megabeds, and were formed by catastrophic events flushing enormous amount of sediment trapped in a proximal deltaic environment (Starek et al. 2013). The Huty Fm. continuously passes into rhythmically-bedded turbidites of the Zuberec Fm., a.k.a. the Chocholów Beds. In places

the Zuberec Fm. is formed by more sand-rich deposits of the Kežmarok Mb. (Gross 1998). The sedimentary sequence of the CCPB is terminated by the Biely Potok Fm. a.k.a. the Ostrysz Fm. composed prevailingly of thick amalgamated sandstone beds. A more distal development of the Biely Potok Fm., the Brzegi Beds, is known from the eastern part of the Podhale Basin (Watycha 1959; Olszewska & Wieczorek 1998; Gedl 2000; Garecka 2005). Deposits of the Zuberec and Biely Potok Fms represent various facies associations of sand-rich submarine fans (Westwalewicz-Mogilska 1986; Wieczorek 1989; Janočko et al. 1998; Starek et al. 2000; Soták et al. 2001; Starek & Fuksi 2017a, b).

Sampling and methods

The sedimentary rocks studied belong to the Tomášovce Mb. of the Borové Fm. (2 sites), Huty Fm. (19 sites), Zuberec Fm. (13 sites) and to the Biely Potok Fm. (3 sites) (Figs. 1C, 2; Supplementary Table 1). The standard sedimentological investigation involved recording of bed thicknesses, grain sizes, sedimentary structures, and the analysis of paleocurrent markers. The paleoflow orientations in the studied deposits were obtained by measurements of erosional structures on bed soles (flute casts, groove marks, tool marks, etc.). Occasionally, structures such as a parting lineation on the upper bed planes were also measured. In total, 222 paleoflow orientations were measured at 38 sites (Fig. 3), either directly on the beds sampled for magnetic anisotropy measurements or on the nearest available beds. The evaluation of the paleoflow orientations was performed by using Orient 3 software (Vollmer 2015). The orientations of paleoslopes were inferred from the orientation of overturned limbs of slump folds and of slump fold axes. Paleoflow orientations were restored to their original pre-tilting orientation by simple tilt correction along the bedding strike. Tectonic features, prevailingly joints, faults and folds, were recorded at each sampling site in order to compare their orientations with the observed magnetic fabric.

Oriented samples for the magnetic fabric study were collected by using a portable gasoline-powered water-cooled drill at 19 sites including individual outcrops or more or less continuous sections distributed throughout the northern and northeastern part of the CCPB in Slovakia. The drill cores were sliced to standard size paleomagnetic specimens by a wheel saw in the laboratory. Additionally, 17 sites studied previously by Márton et al. (1999, 2009a) (Fig. 1C, Supplementary Table 1) were revisited for measuring paleoflow directions and structural features.

For the new magnetic anisotropy study, 4–12 samples were drilled from each bed consisting of one or more turbidite facies (Ta–Te intervals *sensu* Bouma 1962). At sites where samples were collected from mudstones also for paleomagnetic study (in preparation), 3–8 samples from 2–4 beds covering a few metres of an outcrop were drilled. Each sample was oriented individually with a magnetic compass. Magnetic susceptibility and AMS were measured on 459 specimens (Supplementary Table 1) by using a KLY-2 kappabridge (Agico Ltd., former Geofyzika n.p. Brno, the Czech Republic). The site mean tensors were evaluated with Anisoft 4.2 program (Jelínek 1977, 1978; Hrouda et al. 1990; Chadima & Jelínek 2008).

From each interval of the Ta–Te turbidite facies at least 5 samples were selected for the measurement of anisotropy of anhysteretic remanent magnetization (AARM) in order to discriminate the ferromagnetic s.l. sub-fabric from the bulk AMS (i.e. the contribution of all dia-, para- and ferromagnetic s.l. particles). For the AARM experiments a LDA-3A demagnetizer accompanied by a AMU-1 anhysteretic magnetizer (both Agico Ltd., the Czech Republic) were used. The specimens were demagnetized at 100 mT alternating field (AF) and then magnetized at 80 mT AF and 50 μT direct field (DF) in 12 positions (Jelínek 1993). After each magnetization step, the remanence was measured by a JR-5A spinner magnetometer (Agico Ltd., the Czech Republic). The data were computed with the AREF program (Jelínek 1993). The site means were evaluated with Anisoft 4.2 program (Jelínek 1977, 1978; Hrouda et al. 1990; Chadima & Jelínek 2008).

Magnetic mineralogy experiments involved the acquisition of isothermal remanent magnetization (IRM) followed by thermal demagnetization of the three-component IRM (Lowrie 1990). IRM was imparted on selected representative specimens by using a Molspin pulse magnetizer (maximum field 1 T). All anisotropy measurements and magnetic mineralogy experiments were carried out in the paleomagnetic laboratories at the Earth Science Institute of the Slovak Academy of Sciences in Banská Bystrica, Slovakia and at the Mining and Geological Survey of Hungary in Budapest.

In order to reveal microtextures helpful to elucidate the origin of magnetic minerals, and therefore the origin of magnetic sub-fabrics, 12 thin sections from selected samples were prepared for optical microscopy and scanning electron microscopy (SEM). Thin sections for SEM were polished and carbon-coated. SEM observations and energy-dispersive spectra (EDS) analyses were performed on a JEOL JXA-8530FE microprobe with accelerating voltage 15 kV, probe current 20 nA, probe diameter 2 μm, counting time 10 s on peak and 5 s for background. To trace the elemental distributions of iron, sulphur and oxygen for the investigated (para-, ferro-) magnetic minerals, aiding to reveal processes controlling their formation and/or transformation, we performed a compositional mapping by using a wavelength-dispersive spectrometer (WDS). A map of 600×400 pixels was generated with acceleration voltage fixed at 15 keV, probe current at 20 nA, the beam and step size at 200 nm and dwell time at 100 ms. Electron probe micro-analysis (WDS) of pyrite was performed with the following conditions: accelerating voltage 20 kV, probe current 15 nA, beam diameter 2 μm and ZAF matrix correction was used. The EPMA was calibrated by the natural and synthetic standards. Used standards, X-ray lines are: Fe (Kα) – pyrite, As (Lβ) – arsenopyrite, S (Kα) – pyrite, Cu (Kα) – chalcopyrite, Co (Kα) – cobaltite, Ni (Kα) – NiS. All petrographic analyses were carried out in the Laboratory of Electron Microanalysis in Banská Bystrica, Slovakia.

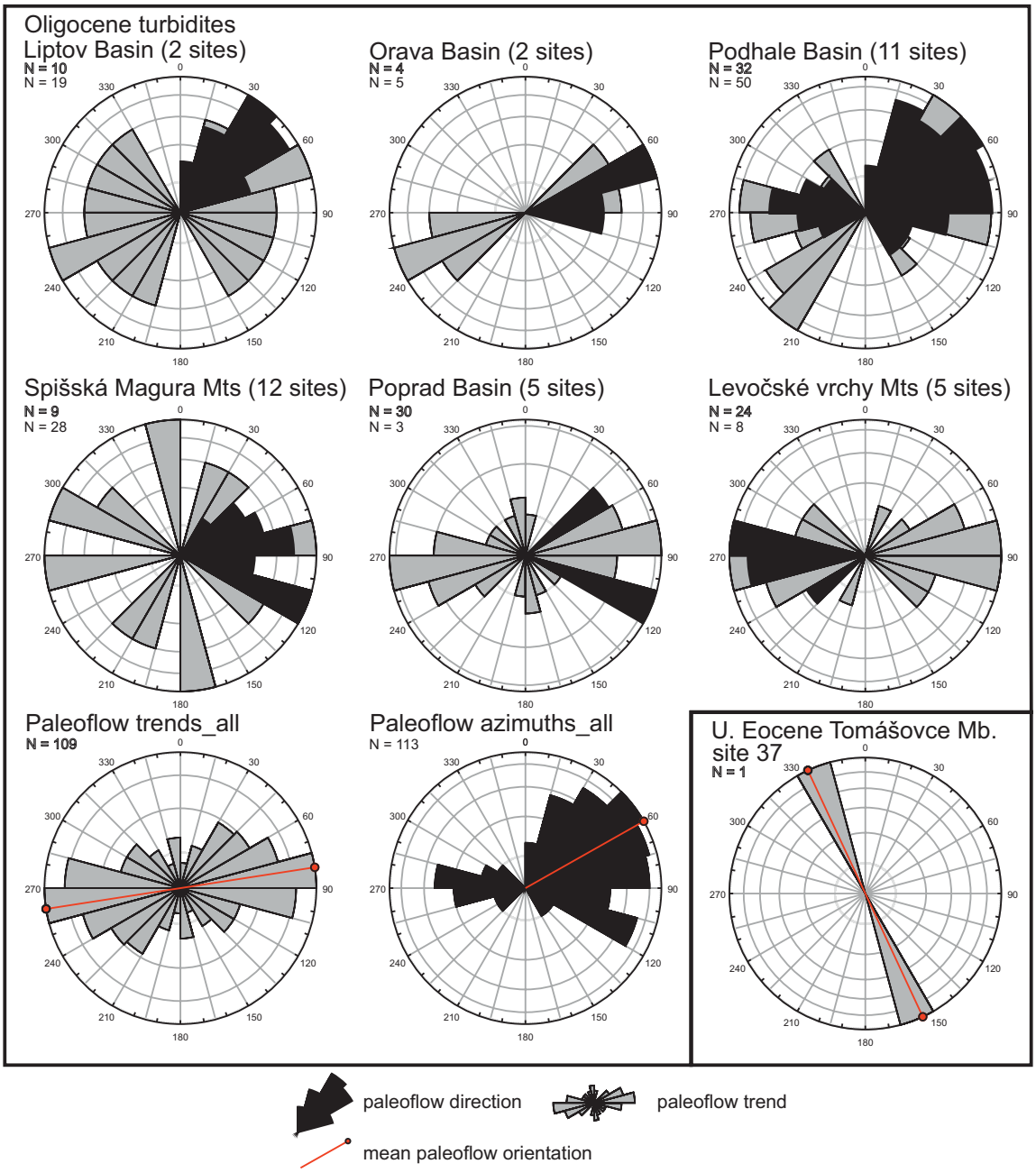

Fig. 3. Rose diagrams showing paleoflow orientations after tectonic corrections measured at 38 sites from the Oligocene/earliest Miocene turbidite deposits and at one site from Upper Eocene fluvio-deltaic sandstones of the Tomášovce Mb. Diagrams are divided for individual sub-basins in northern and north-eastern parts of the CCPB (for location see Fig. 1C).

Results

Paleoflow orientations

In the Upper Eocene fluvio-deltaic deposits of the Tomášovce Mb. (studied at sites 35 and 37, see Figs. 1C, 2, Supplementary Table 1) the SSE–NNW trend of paleoflows was observed (Fig. 3). The pebble material from intercalating conglomerate beds suggests southerly (in present coordinates) source areas composed of crystalline and sedimentary rocks of the Central Western Carpathian tectonic units (Marschalko 1966; Filo & Siráňová 1996, 1998). Within the Oligocene turbidite deposits (the Huty, Zuberec and Biely Potok fms.) the paleoflow directions are quite consistent through the sequence (Fig. 3). Regardless of some variations at site level, the paleoflows keep the general WNW–ESE to WSW–ENE trend with directions prevailingly towards E and NE in the Liptov, Orava and Podhale Basins (cf. Králiková et al. 2014; Starek & Fuksi

2017a,b; Starek et al. 2019). Occasionally, opposite reverse directions from E to W were also measured (cf. Starek et al. 2019). In the Spišská Magura Mts. and in the Poprad Basin the WSW–ENE to WNW–ESE directions prevail but occasionally the NNW–SSE trend was observed. In the eastern part of the CCPB, in the Levočské vrchy Mts., the E–W trend of paleoflows was measured (Fig. 3). It is in line with the previously reported W-ward directed paleoflows (Janočko et al. 1998; Soták et al. 2001).

Magnetic mineralogy

The mean magnetic susceptibility (Km) ranges from 111 to 365×10^{-6} SI (mean $218.9\pm53.5\times10^{-6}$ SI) in mudstones and from 66 to 252×10^{-6} SI (mean $139.5\pm41.1\times10^{-6}$ SI) in sandstones (Fig. 4). The identification of the magnetic minerals was attempted by IRM acquisition experiments followed by thermal demagnetization of the three orthogonal IRM components acquired in fields of 0.12, 0.36 and 1 T, respectively (Lowrie 1990). These experiments showed that the magnetic minerals were fast saturating in both sandstone and mudstone facies (Fig. 5). The demagnetization curves revealed that the dominant component is represented by the coercivity lower than 0.12 T. This component continuously decays up to the 580°C (Fig. 5), which suggests the presence of fine-grained magnetite (cf. Márton et al. 2009a). Magnetic mineralogy experiments performed by Hrouda et al. (2018) indicate wider grain size range of single- to multi-domain slightly non-stoichiometric magnetites in sandstones. The rise of the susceptibility above 400 °C can be related to the decomposition of iron sulphides, weakly indicated also by the decay of the medium coercivity component by 400 °C.

SEM observations

In seven representative samples selected (Fig. 6) ferromagnetic minerals s.l. have not been directly identified by means of the SEM observations. The presence of trellis structures in some grains (Fig. 6A) with Ti-rich exsolution lamellae and completely dissolved Fe-rich domains suggests a complete dissolution of detrital Fe–Ti oxides during diagenesis. In this regard, the ubiquitous presence of paramagnetic iron sulphide, pyrite (cf. Márton et al. 1999, 2009a), is remarkable because of its potential as a prerequisite mineral for neoformation of ferromagnetic phases during early or late diagenesis (Kodama 2012 and references therein). The SEM investigation revealed at least two generations of pyrite (Fig. 6B–G). Pyrite, occurring as spherical framboids up to 10 μm composed of euhedral grains up to 1 μm in size (Fig. 6B–E), is typical for early diagenetic reduction processes (Roberts & Weaver 2005). Cryptocrystalline pyrite (Fig. 6C,D) or euhedral pyrite grains in micron/submicron sizes (Fig. 6E, F), both surrounding larger framboids, represent younger pyrite generation(s). The occurrence of pyrites is restricted mostly to carbonate cement (Fig. 6E, F), clay matrix or to voids filled by organic matter (Fig. 6G). Iron sulphides were also identified on cleavage planes of phyllosilicate minerals such as muscovite or chlorite (Fig. 6H). It was difficult to correctly determine the exact Fe:S ratio of the iron sulphides, and therefore distinguish between pyrite, greigite or pyrrhotite, because the sizes of crystals are at the precision limit of the microprobe with likely element contamination from the host iron bearing chlorites. However, prismatic habit of the iron sulphides within phyllosilicate minerals suggest pyrrhotite (Fig. 6H).

Finer-grained phyllosilicate minerals and associated iron sulphides are not distributed equally but are concentrated within laminae aligned parallel to the bedding. In particular depositional intervals (e.g. ripple cross-laminated sandstones, convoluted sandstones) the laminae represent either cross-laminated ripples oriented oblique to the bedding plane or the laminae are contorted or folded due to a syn- or early post-sedimentary soft-sediment deformation (Fig. 6I).

Large amounts of pyrites occur in places. On the other hand, calcite veins are devoid of pyrite or any opaque mineral. Dolomite crystals with iron rich rims were frequently observed as a part of carbonate cement. Occasionally, paramagnetic iron carbonate, siderite, was identified.

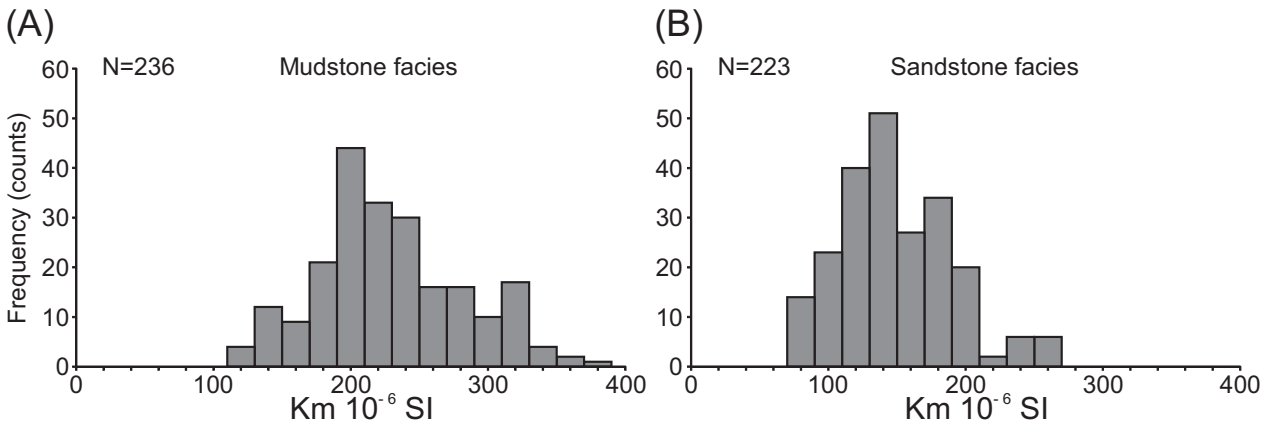

Fig. 4. Frequency distribution of the mean susceptibility Km shown individually for mudstone (**A**) and sandstone facies (**B**).

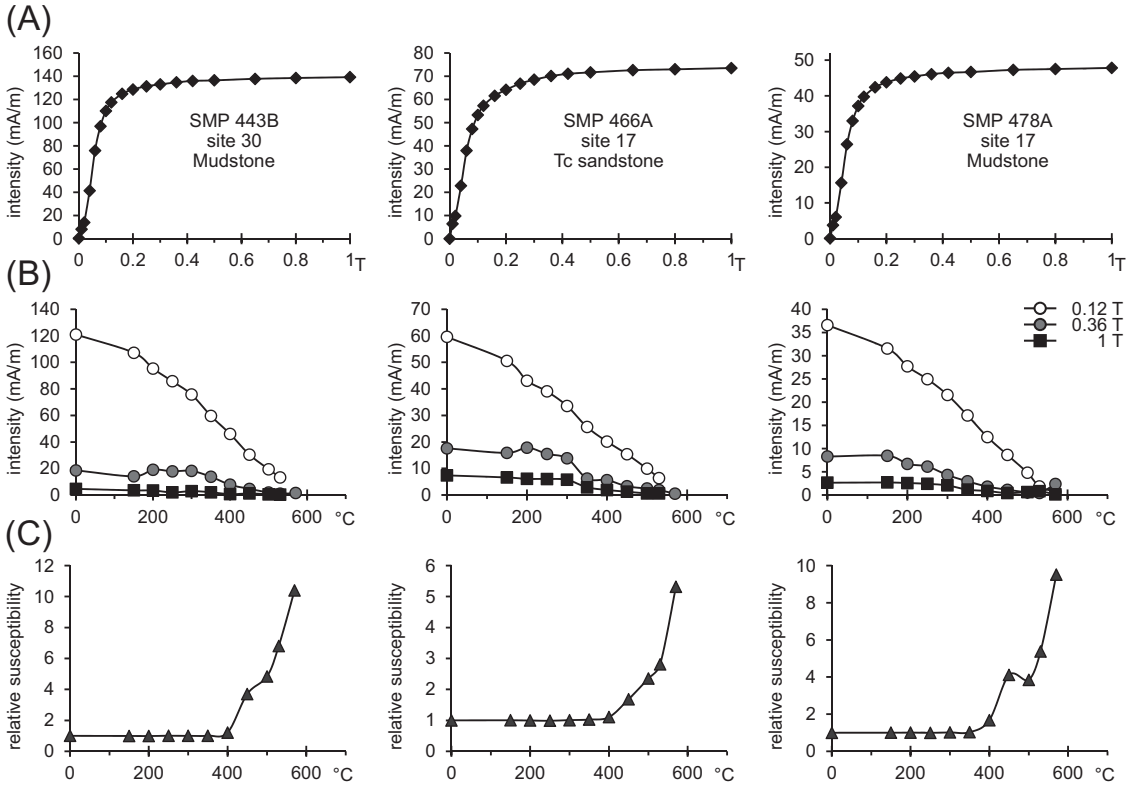

Fig. 5. Magnetic mineralogy of the analysed samples. **A** — Isothermal remanent magnetization (IRM) acquisition curves; **B** — the 3-component IRM thermal demagnetization; **C** — magnetic susceptibility monitored during heating. The hard (squares), medium hard (dots) and soft (circles) components of the IRM were acquired at 1 T, 0.36 T and 0.12 T, respectively.

The compositional distribution mapping showed that the darker zones surrounding the pyrite crystals (Fig. 6C,D) and framboids (Fig. 7A) reflect distinct composition of iron and sulphur in the rims (Fig. 7B,C). The rims are characterized by the decrease of iron and sulphur (cf. Kars et al. 2014), while the oxygen content increases at the rims and at the surface of the pyrite crystals (Fig. 7D). To prove the presence of different generations of pyrite and oxidation processes the euhedral grains of pyrite (Fig. 6C,D) were measured on a microprobe (WDS analyses). The lighter zones on BSE images (Fig. 6C,D), representing mainly cores of grains, correspond to stoichiometric pyrite with a crystallochemical formula based on 3 apfu to $FeS_{2.00}$. The darker zones surrounding the cores show decreased content of Fe. The analyses have lower totals (97–97.8 wt. %) and the crystallochemical formulae can be expressed as $Fe_{0.97}S_{2.00}$. The decreased iron content is balanced with oxygen, which is clearly visible from the compositional maps (Fig. 7) and was confirmed and quantified by EDS analyses (~3.4 wt. %).

Turbidite facies and AMS

The anisotropy degree Pj (Jelínek 1981) in sedimentary rocks is usually up to <1.05 (Tarling & Hrouda 1993; Hrouda et al. 2009). In the studied material it is somewhat higher: in mudstones Pj<1.16 (mean 1.089±0.040), in sandstones Pj<1.07 (mean 1.029±0.013) (Fig. 8A). The shape of anisotropy ellipsoid is mostly oblate to triaxial and occasionally slightly prolate (Fig. 8B). Magnetic fabric is well-developed (Fig. 9) with magnetic foliation oriented subparallel with the bedding planes and the magnetic lineations are quite well-grouped on regional as well as site levels (Fig. 9).). In general, there is a common orientation of the AMS fabric, yet slight to significant differences between the Ta–Te intervals *sensu* Bouma (1962) on the turbidite facies were observed (Fig. 10).

Massive or normally graded sandstones – Ta

Massive or normally graded sandstones were collected at 8 sites (10 beds, 59 samples, Fig. 9, Supplementary Table 1). They are represented by fine-grained to medium-grained sandstones mostly without visible structures (Fig. 10A). Normal gradation sporadically developed. Most frequently, the massive sandstones occur as the lowermost parts of thicker (15–25 cm) beds overlain by parallel-laminated intervals.

The minimum susceptibility axes (Kmin) are oriented near the bedding poles. Magnetic lineations (Kmax) are well-grouped and oriented WSW–ENE, parallel to the flow orientations measured on the sampled beds or on the nearest available beds (Fig. 9).

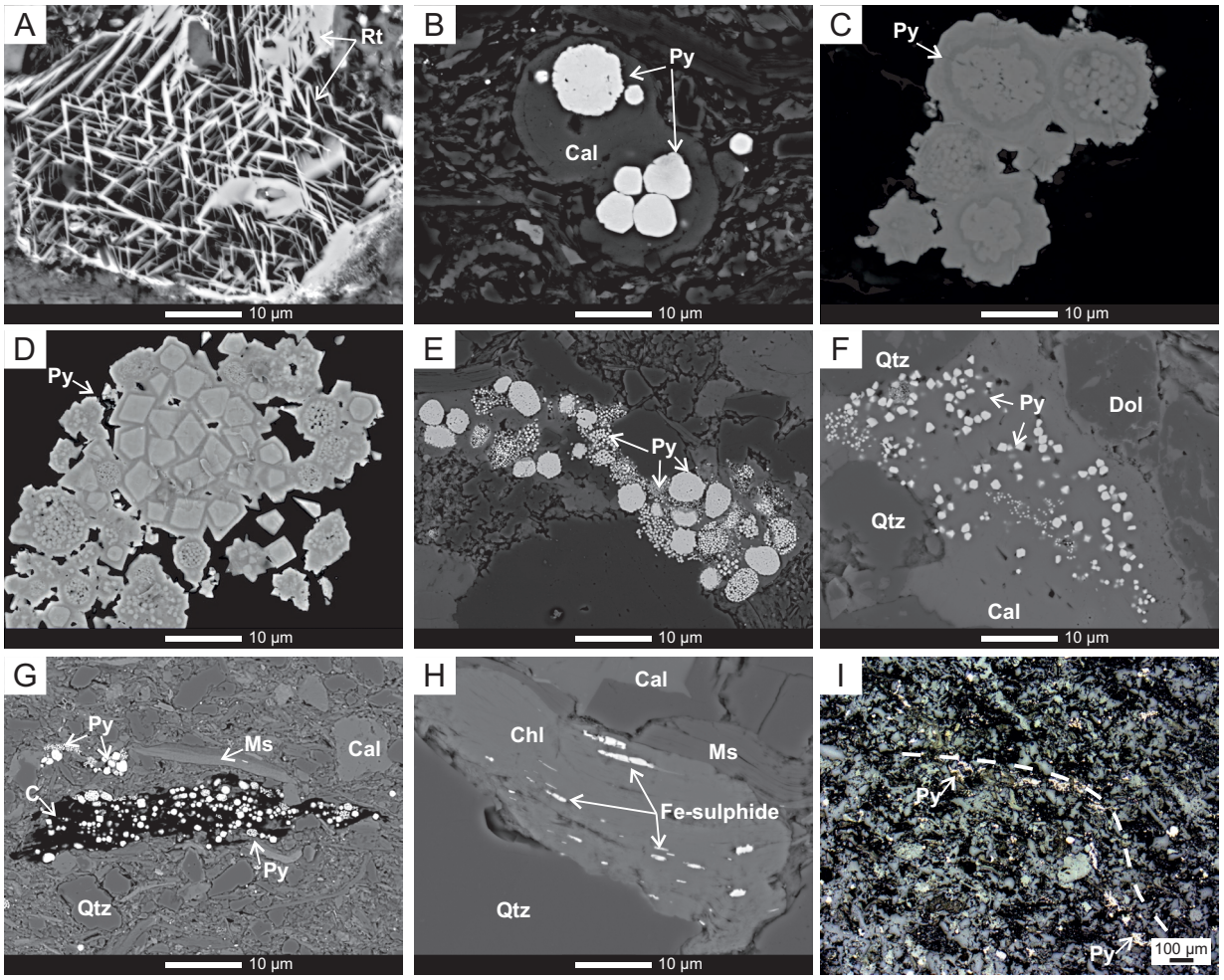

Fig. 6. Back-scattered images of representative samples. **A** — Trellis structures in strongly altered Fe–Ti oxide grain, black domains between bright Ti-rich lamellae represent now completely dissolved, formerly Fe-rich domain, sample LM23, site 2; **B** — spherical framboids composed of euhedral pyrites, note calcite surrounding framboids suggesting early diagenetic origin of pyrite, sample SMP419, site 30; **C, D** — pyrite framboids and large euhedral pyrite crystals surrounded by cryptocrystalline pyrite, sample SMP506, site 21; **E** — several generations of small micron/submicron pyrite crystals surrounding larger pyrite framboids in carbonate cement, sample SMP431, site 30; **F** — two generations of pyrite crystals within calcite cement, sample SMP431, site 30; **G** — pyrite crystals and framboids concentrated in black organic matter filling voids between detrital quartz, calcite and micas, sample SMP419, site 30; **H** — iron sulphide within cleavage plains of chlorite grain, note the prismatic habit of iron sulphides suggesting pyrrhotite, sample SMP431, site 30; **I** — pyrite concentrated mostly in the hydroplastically deformed lamination composed of finer-grained clay minerals, the dashed line marks the lamination, sample SMP506, site 21, the image taken under reflected light. Abbreviations for minerals according to Whitney & Evans 2010.

Parallel-laminated sandstones – Tb

Parallel-laminated sandstones represent fine- to medium-grained sandstones which constitute either a part of repetitive Ta–Tb or Tb–Tc intervals within one bed (Fig. 10B,C) or the entire bed consists of the planar lamination (Fig. 10D). The planar lamination comprises mm-thick individual laminae. The lower parts of the beds are often sharp with erosional contacts and well-developed sole marks (Fig. 10B). The parallel-laminated sandstones were sampled at 6 sites (13 beds, 87 samples, Fig. 9, Supplementary Table 1).

The magnetic fabric is characterized by Kmin perpendicular or gently inclined to the bedding. The well-grouped magnetic lineations are mostly oriented WSW–ENE, parallel to the flow orientations (Fig. 9). Occasionally the Kmax are oriented oblique or perpendicular to the flow orientations.

Ripple cross-laminated sandstones – Tc

Ripple cross-laminated sandstones were sampled only at one site (1 bed, 6 samples, Fig. 9, Supplementary Table 1). They occur mostly in thinner up to 10–15 cm beds (Fig. 10E). The Tc intervals form very frequent repetitions with the Tb parallel-laminated intervals within a single bed (Fig. 10C). The height of the cross-laminated parts was up to 5 cm. Climbing ripple lamination was rarely observed.

The magnetic lineations in cross-laminated sandstones are very well-clustered parallel to the local paleoflow orientation (Fig. 9). The Kmin are situated near the bedding pole.

Convoluted sandstones – Tcv

Fine- to medium-grained sandstones with a convex-upward lamination, sometimes slightly overturned lamination and/or concave-upward dish structures are regarded here as convoluted sandstones. Convolutions continuously develop mostly from ripple cross-laminated or parallel-laminated parts or alternate with them (Fig. 10F,G). In some cases, where convolutions developed from parallel-laminated sandstones, the convolution crests are oriented parallel or slightly oblique to the sole marks measured on the bottom beds. Samples from the convoluted sandstones were collected at 3 sites (3 beds, 20 samples, Fig. 9, Supplementary Table 1).

The AMS fabric in the convoluted sandstones is less ordered than in the undisturbed Ta–Tb–Tc intervals. Clustering of Kmax varies at different sampling sites from well to poorly clustered. The magnetic lineations are oriented roughly parallel to the paleoflow and to the convolution crest. The Kmin create a small to moderate girdle oriented perpendicular to the Kmax (Fig. 9).

Slump folded sandstones – Tsf

Sandstone beds internally deformed by cm-scale slumping were sampled at two sites (2 beds, 20 samples, Fig. 9, Supplementary Table 1). These beds contain deformation structures such as disharmonic folds often with overturned limbs. The syn-sedimentary origin of the folds is obvious since the folded beds are distributed between non-deformed parallel-laminated or massive mudstone and sandstone beds (Fig. 10H,I). The orientation of slump fold axes follow the local paleoslopes oriented roughly perpendicular to the general paleoflow direction.

The AMS fabric in the slump folded sandstones is different from the AMS fabric in the undisturbed turbidite Ta–Tb–Tc intervals. The magnetic lineations are well-grouped and oriented parallel to the slump fold axes (Fig. 9). The Kmin create a girdle oriented perpendicular to the Kmax.

Massive and parallel-laminated mudstones – Te

Samples from mudstones were collected primarily for paleomagnetic study (in preparation), thus massive mudstones Fig. 10J) without visible lamination were preferred for this purpose. However, such massive mudstone beds were rare,

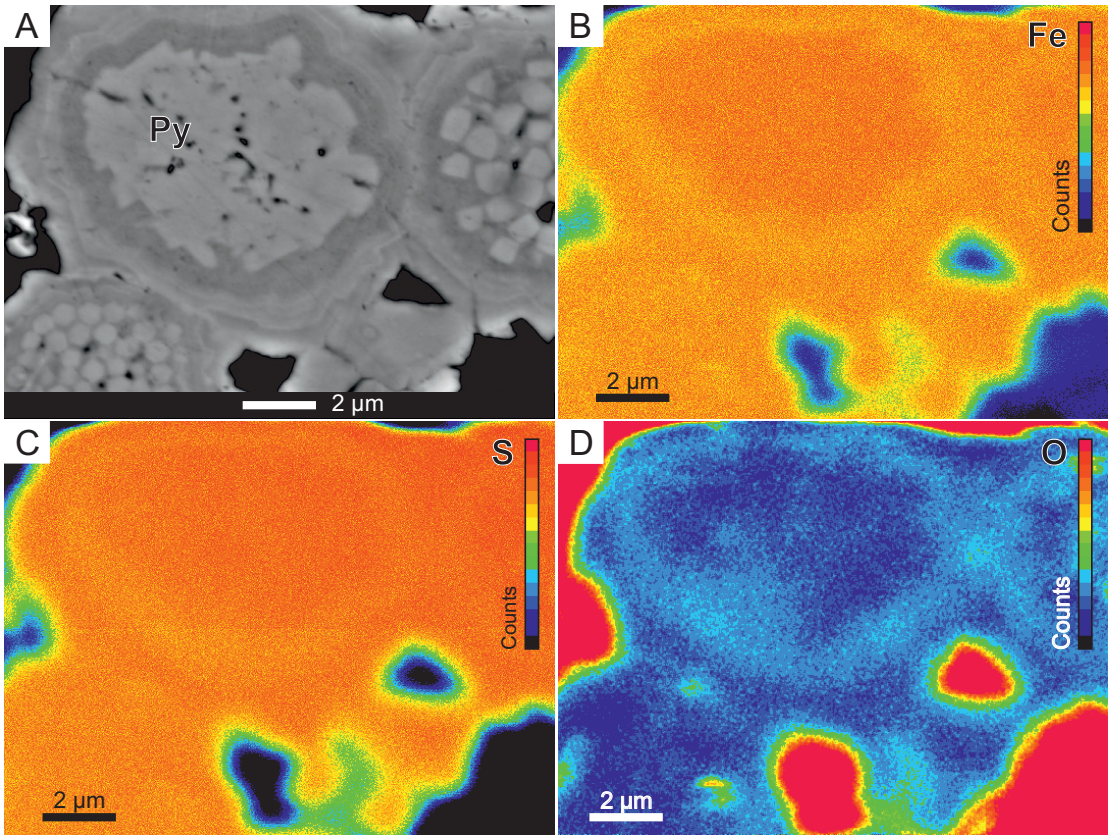

Fig. 7. Compositional distribution maps of iron, sulphur and oxygen for iron sulphide framboids in sample SMP506, site 21. **A** — backscattered image of analysed pyrite framboids; **B** — distribution of iron, note a rim around the pyrite framboid with decreased content of iron; **C** — distribution of sulphur, the rim around the pyrite framboid shows decrease of sulphur; **D** — bright zones of higher oxygen content at the rims and surfaces of pyrite framboids.

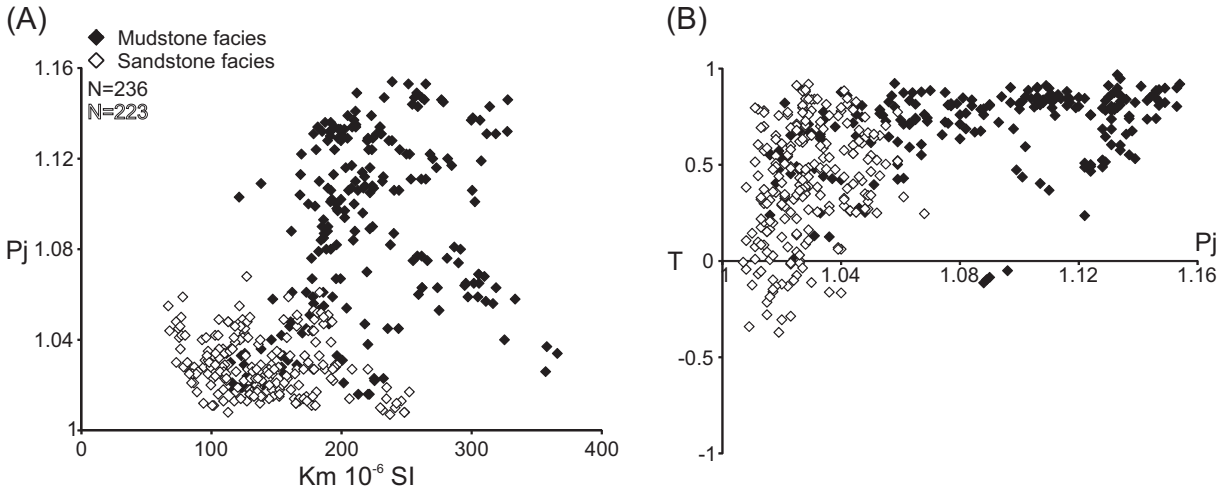

Fig. 8. A — Correlation between the mean susceptibility Km, and the degree of anisotropy Pj; **B** — correlation between the degree of anisotropy Pj, and the shape of anisotropy ellipsoid T, separately for the mudstone and sandstone facies.

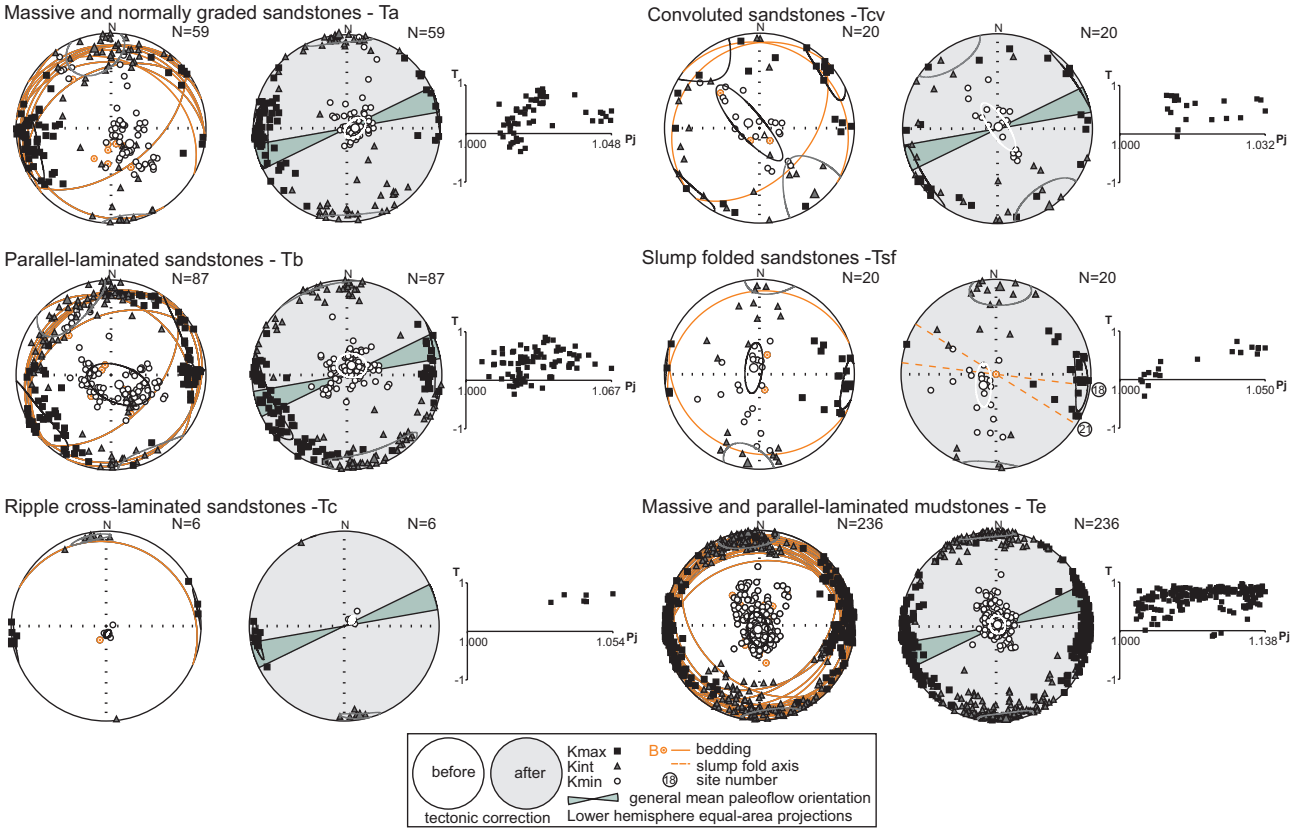

Fig. 9. Stereographic projections of the AMS axes and Pj–T diagrams for different turbidite intervals (Ta–Te intervals sensu Bouma 1962). The green roses constrain confidence regions of the mean general paleoflow direction (72°±8°). The dashed orange lines show the mean trend of slump fold axes for respective sites. Numbers correspond to Fig. 1C and Supplementary Table 1.

therefore, samples were collected mostly from parallel-laminated mudstones (Fig. 10K). The massive mudstones were devoid of visible structures. The parallel-laminated mudstones consist of mm laminae of fine-grained silt material. At one site (site 31, Fig. 1, Supplementary Table 1) well-developed flute marks, as negative casts on the upper bed planes, were observed in parallel-laminated mudstones (Fig. 10L).

The Kmin axes are oriented near the bedding poles. Magnetic lineations are well-grouped around the paleoflow orientations measured on the nearest available sandstone beds

or in one case directly on the mudstone beds (Figs. 9, 10L, 11). Occasionally the Kmax were poorly clustered and dispersed within the bedding plane (Fig. 11, site 20).

Turbidite facies and AARM

To consider a magnetic fabric anisotropic the F test at the 95 % confidence level must be above 3.48. This criterion was satisfied in a few cases for mudstone facies, where the error angles are also within the acceptable limit E12<15. For some other mudstone samples and for all sandstone facies studied the F test was negative, in other words, the fabric was defined as isotropic. Moreover, the error angle E12 was often very large, exceeding 30 (cf. Márton et al. 2009a). Nevertheless, the principal axes of the AARM ellipsoids showed distinct patterns, permitting to distinguish the following types of the ferromagnetic s.l. fabrics (Fig. 12).

AARM Type 1

This type was recognized at two sites (17 and 21, Figs. 1, 12) in the ripple cross-laminated sandstones and in the slump folded sandstones, respectively. In these facies the AARM pattern differs from the AMS fabric (Fig. 12). The minimum anisotropy axes (Amin) are grouped near the poles to the joint sets trending NNW–SSE and NE–SW, respectively. The maximum and intermediate axes of the AARM are distributed along one of the joint planes, which are the NE–SW trending joints at site 17 and the NNW–SSE trending joints at site 21 (Fig. 12).

AARM Type 2a

This type was observed in the mudstones at site 21 (Figs. 1, 12). In this case the Amax is oriented N–S, slightly deflected from the bedding to joint intersection and perpendicular to the Kmax. The Amin coincide with the Kmin and both are situated close to the bedding poles.

AARM Type 2b

The AARM type 2b was observed in the massive and parallel-laminated sandstones at site 2 (Figs. 1, 12). The Amax gently plunging to the NW are oriented almost perpendicular to the Kmax and group close to the joint to bedding intersections (Fig. 12). The Amin coincide with the Kmin. In one case the Amin interchanged its position with the Aint (Fig. 12).

AARM Type 3

The AARM type 3 was revealed in the convoluted sandstones at site 30 (Figs. 1, 12). This type is oriented similarly to the AARM type 2b at site 2, but unlike that, the AARM fabric of this type roughly coincides with the AMS fabric. The Amax are slightly better grouped than the Kmax.

Discussion

Origin of the AMS fabrics

In sedimentary rocks where magnetic susceptibility does not exceed 5×10^{-4} SI (Tarling & Hrouda 1993) (Figs. 4, 8) the AMS fabric has often been interpreted as basically reflecting the preferred orientation of paramagnetic minerals with very small contributions from ferromagnetic s.l. minerals (Rochette 1987; Cifelli et al. 2009). X-ray diffraction investigation identified dia- and paramagnetic minerals (clays, chlorite) as the main constituents of the studied rocks (Środoń et al. 2006) and the SEM investigations found few indications for ferromagnetic s.l. phases. Low temperature variation of susceptibility shows dominant paramagnetic hyperbola, documenting that paramagnetic susceptibility contributes to the total bulk susceptibility more than 90 % (Hrouda et al. 2018). Moreover, the orientations of the ferromagnetic s.l. fabrics (AARM) mostly differ from the AMS fabrics (Fig.12). Thus, it is reasonable to suggest that paramagnetic minerals are the main carriers of the AMS.

The AMS ellipsoids are dominantly oblate with magnetic foliation sub-parallel to the bedding, which can be attributed to deposition/compaction processes. The correlation is fairly good between the AMS lineations and W–E to SW–NE oriented general and local paleoflows (Figs. 9, 11). Slight differences between the Kmax and measured paleoflow orientations could be explained by small differences in flow directions during erosive phases, generating sole marks, and final depositional phases of the turbiditity currents in which massive, planar and cross-planar structures formed (Felletti et al. 2016). Deviations up to several tens of degrees from a flow direction might be caused by the spatial variations in current directions due to several factors, like incomplete reorientation of rolling (flow-perpendicular) fabric to flow-aligned fabric and vice versa, changes in bed roughness and post-sedimentary deformation such as bioturbation, fluidization or soft-sediment deformation (Bass et al. 2007).

In spite of the strong arguments in favour of the sedimentary origin of the AMS lineations, the alternative possibility of their deformation origin also has to be considered, since the studied sediments clearly show evidence for tectonic deformation due to basin inversion. In a compressional stress field, the first expected response to deformation is the layer parallel shortening producing an AMS lineation sub-parallel to the bedding strike (roughly perpendicular to the maximum compression) while the Kmin remain near the bedding pole (Tarling & Hrouda 1993; Parés et al. 1999; Hrouda et al. 2009; Soto et al. 2009; Almqvist & Koyi 2018). In order to investigate the possibly deformational origin of the AMS lineations, we were able to make direct comparisons for 12 sites (sandstone beds bearing reliable flute casts) between the AMS lineations and the bedding strikes on one hand, and between the AMS lineations and the paleoflow directions, on the other hand. This leads to the conclusion that the AMS lineations must be of sedimentary origin, due to the poor correlation between the local

strike and magnetic lineations (Fig. 13A) and the good positive correlation between the AMS lineations and local paleoflows in the Ta–Tb–Tc intervals (Fig. 13B).

The sedimentary origin of the AMS fabrics is further supported by the following observations: (1) In the Upper Eocene fluvio-deltaic sandstones of the Tomášovce Mb. the AMS lineations are oriented differently to the magnetic lineations of the Oligocene turbidites (Figs. 3, 14) and coincide with the measured NNW-N directed paleoflows (Marschalko 1966; Filo & Siráňová 1996, 1998). (2) In the hydroplastically deformed facies such as convolute and slump folded sandstones the AMS fabrics (Fig. 9) correspond well with the soft-

Fig. 10. Sedimentary facies and structures observed at the outcrops studied. For location see Fig. 1C and Supplementary Table 1. **A** — Massive structureless fine-grained sandstone, site 28; **B** — parallel-laminated fine- to medium-grained sandstone with well-developed sole marks (pointed by arrow) at the bottom beds, site 5; **C** — repetitions of parallel- and ripple cross-laminated intervals in the sandstone bed, site 5; **D** — parallel-laminated sandstone, the most frequent sandstone facies studied, site 5; **E** — ripple cross-laminated sandstone bed, site 17; **F, G** — convolutions developed above the cross-laminated or parallel-laminated part of the bed, F at site 30, G at site 5; **H** — hydroplastically deformed sandstone bed situated between non-deformed parallel-laminated mudstones, the white rectangle marks the position of the close-up shown in I, site 21; **I** — overturned limbs of syn-sedimentary folds (dashed line) above the non-deformed parallel-laminated sandstone; **J, K** — massive and parallel-laminated mudstones occur as 10–100 mm thick beds alternating with sandstone beds, J at site 30, K at site 5; **L** — flute marks as negative casts on the upper bed planes of mudstones, site 31.

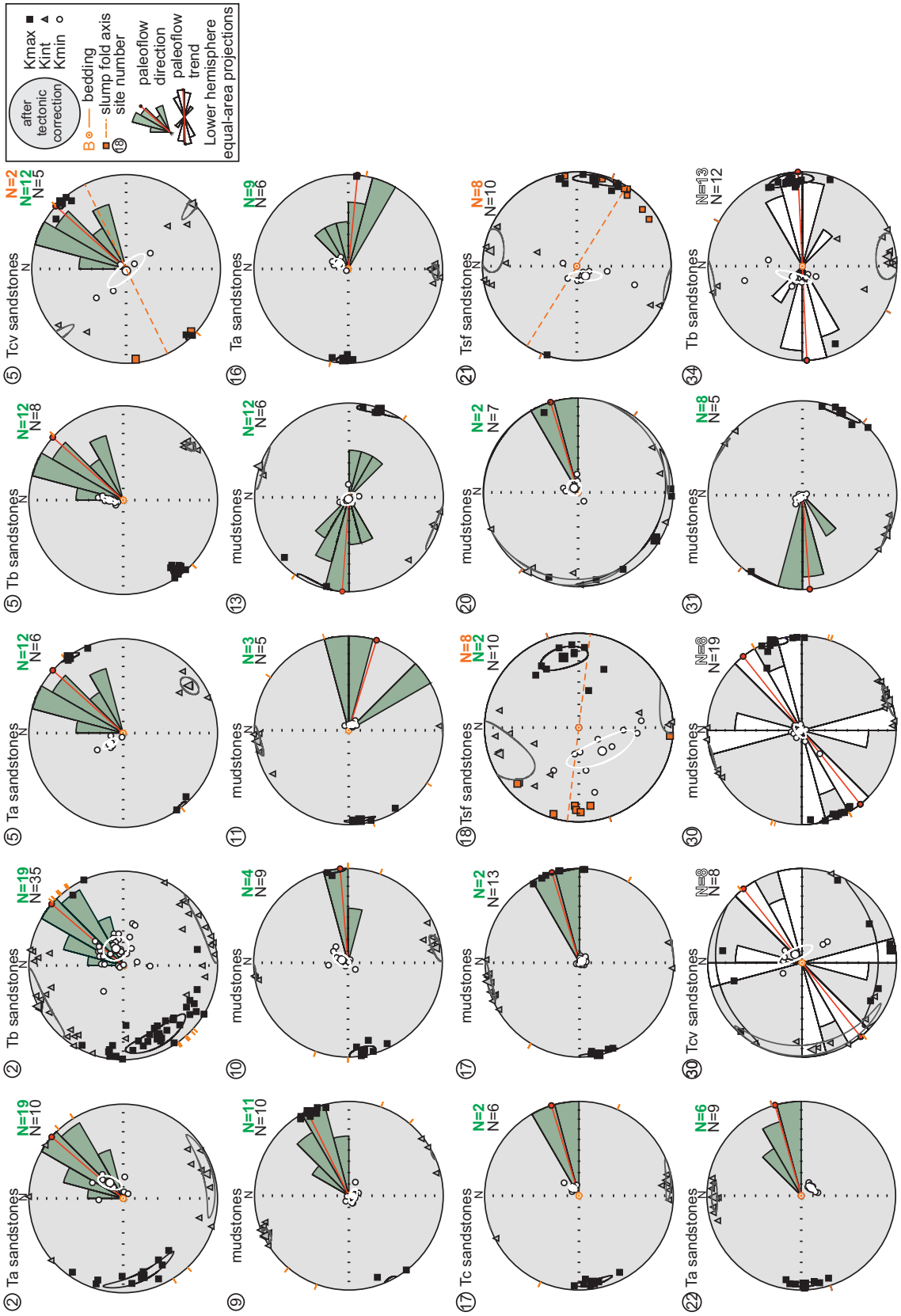

Fig. 11. Stereographic projections of the AMS axes after tectonic corrections at selected sites, where reliable paleoflow directions/trends (green/white rose diagrams) were measured. The orange rectangles and the dashed lines show slump fold axes or convolution crests orientations with the mean trend, respectively. Numbers in circles correspond to the sites in Fig. 1C and Supplementary Table 1.

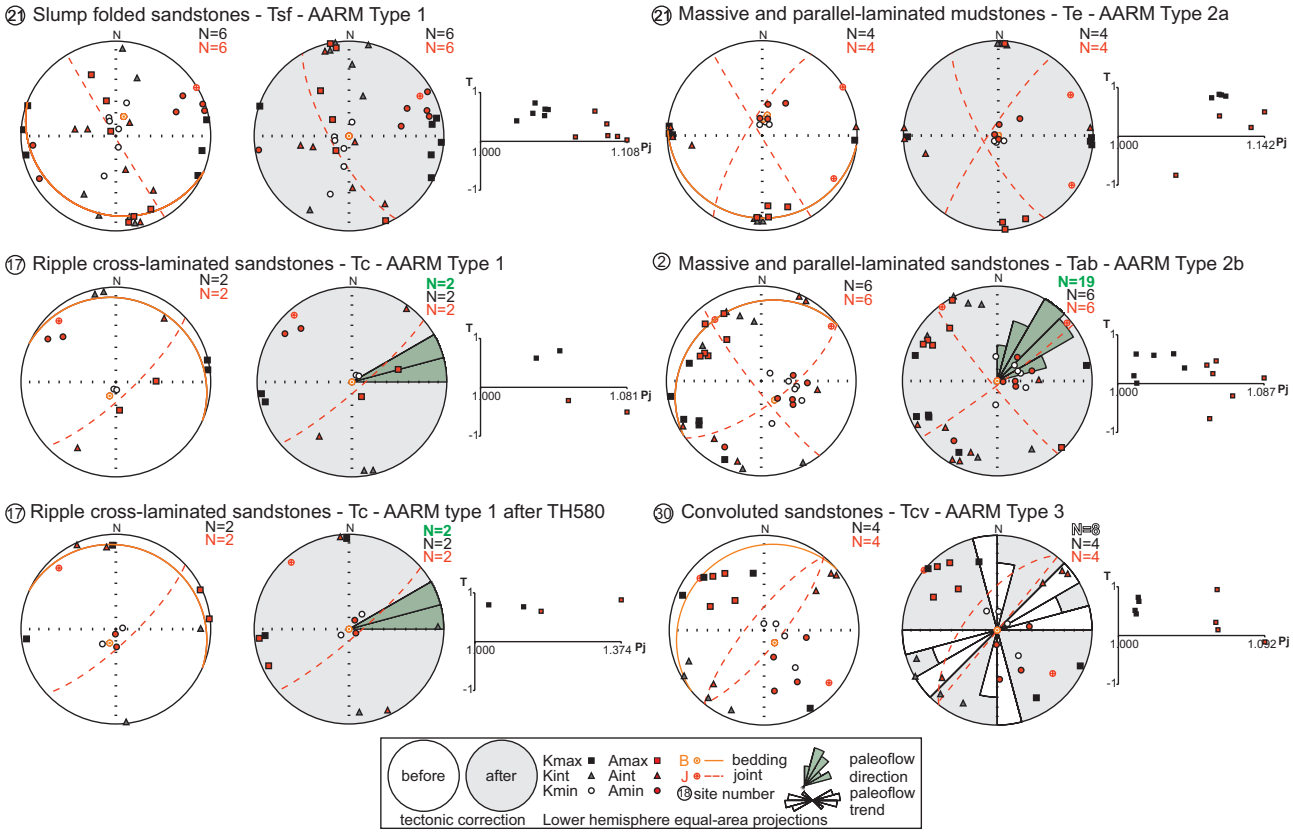

Fig. 12. Comparison of the orientation of the AARM (red symbols) and AMS fabric (black, grey and white symbols) at the site level for different turbidite facies. Left/right diagrams before/after tectonic correction. Joint sets or faults measured at the sampling sites are shown by the red dashed lines. White/green rose diagrams on the stereograms after tectonic correction show paleoflow trends/directions measured directly at or close to the sampling sites. Numbers in circles correspond to the sites in Fig. 1C and Supplementary Table 1. Stereograms are accompanied by Pj–T diagrams.

sediment deformation structures. The magnetic lineations correlate with the slump fold axes/convolution crests and the Kmin create a girdle perpendicular to it (Figs. 9, 11). This magnetic fabric formed during slumping on an unstable depositional slope when the sediment was still wet and poorly lithified (cf. Schwehr & Tauxe 2003; Pueyo Anchuela et al. 2011).

For the mudstone facies, the good correlation between Kmax and the local paleoflow directions measured on the intercalated sandstone/mudstone beds (Figs. 9, 11) also provides a proof for the sedimentary origin of the AMS lineation. The studied mudstones were mostly deposited by genetically related dilute turbidite flows generating coarser-grained facies rather than from the (hemi-) pelagic settling from the water column between flow events (cf. Dall'Olio et al. 2013), although scattered lineations within the bedding planes were also observed (Fig. 11, site 20).

Origin of the AARM fabrics

Origin of the ferrimagnetic minerals

In most of the studied cases, the AARM fabrics were oriented differently from the AMS fabrics. The former seem to be related to a common network of diagonal joints (Fig. 12). In this regard, it is important to discuss the origin and formation time of the ferrimagnetic minerals carrying the AARM fabrics.

The network of several medium to widely spaced sub-vertical diagonal joints striking NNW–SSE (NW–SE) and NE–SW, respectively, is the ubiquitous feature throughout the northern part of the CCPB (Ludwiniak 2010, 2018; Ludwiniak et al. 2019 and references therein). The joints are often opened and filled with several generations and types of calcite and quartz crystals (Hurai et al. 1995, 2002, 2006). Methane fluid inclusions trapped in the blocky and drusy quartz crystals infer a crack-sealing mechanism of the joint formation during upward and lateral migration of hot-methane-rich fluids in the CCPB (Hurai et al. 1995, 2002, 2004, 2006). Calculated PT conditions point to 130–205 °C temperature and 0.5–1.5 kbar pressure during the methane liberation caused by thermal decomposition of organic matter due to burial (Hurai et al. 1995, 2002, 2004, 2006). The reported PT values correspond in the western part of the CCPB to the 2–3 km (90–100 ºC) and up to 5.3–6.5 km (130–205 ºC) depth of burial in the Spišská Magura Mts., in the east (Hurai et al. 2004; Środoń et al. 2006). Isotopic K–Ar dating of the clay

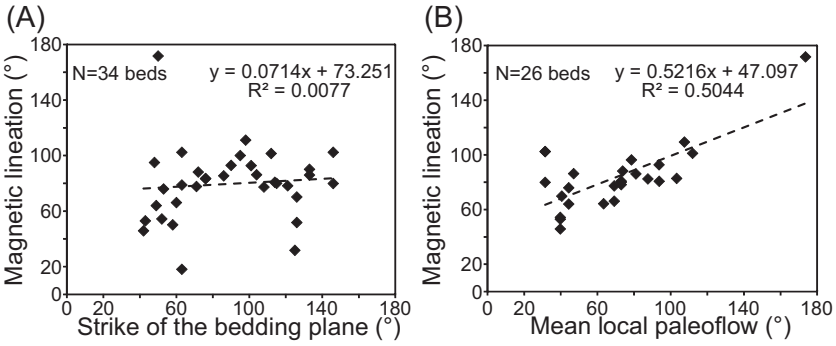

Fig. 13. Comparison between magnetic lineations, strike of the bedding planes and paleoflow directions at 12 sites. **A** — comparison between magnetic lineations and strike of the bedding planes for 34 sandstone beds; **B** — good positive correlation between the magnetic lineations and local paleoflows measured on 26 sandstone beds.

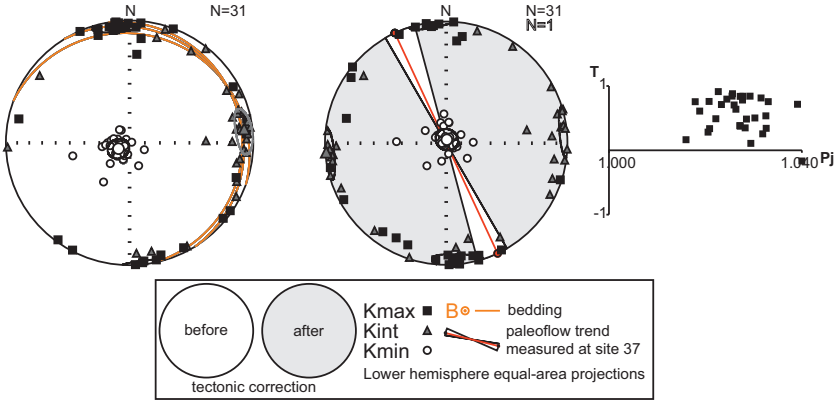

Fig. 14. Stereographic projections of the AMS axes and Pj–T diagrams for fluvio-deltaic sediments of the Upper Eocene Tomášovce Mb. of the Borové Fm (sampled at sites 35, 37). The white rose diagram on the stereogram after tectonic correction shows the paleoflow trend measured at site 37 (for location see Fig. 1C and Supplementary Table 1).

fractions <2 μm revealed that the maximum burial of the CCPB was reached very quickly due to a rapid sedimentation rate close to the incipient inversion of the basin at ~16–19 Ma (Środoń et al. 2006). These values fit well the conditions required for the late diagenetic formation of ferrimagnetic iron oxides/sulphides in non-metamorphic fine-grained deposits (Aubourg & Pozzi 2010; Aubourg et al. 2012). Consequently, the ferrimagnetic minerals carrying the AARM fabrics could form at the same time as the joints.

The growth of ferrimagnetic minerals during burial can be basically related to the clay transformation processes (Katz et al. 1998) or to the oxidation of pyrite crystals (Suk et al. 1990; Elmore et al. 2012). A characteristic feature for the Oligocene deep-water deposits of the CCPB is the relatively high content of paramagnetic iron sulphide, pyrite (Márton et al. 1999, 2009a). The SEM observations of the present study revealed several generations of pyrite indicating their different formation time during diagenesis (Fig. 6). Compositional mapping and WDS analyses revealed oxidized rims surrounding both pyrite framboids and euhedral pyrite grains (Fig. 7). This has been observed in several remagnetized rocks (Suk et al. 1993; Banerjee et al. 1997; Jiang et al. 2001; Kars et al. 2014). Although, ferrimagnetic minerals were not observed directly, submicroscopic ferrimagnetic phases are assumed to be present at the rims of the pyrite grains. Therefore, the late diagenetic pyrite alteration and neoformation of ferrimagnetic minerals is very likely. We observed iron (ferrimagnetic?) sulphides also within phyllosilicate minerals (Fig. 6H), thus clay transformation processes could be involved as well (Katz et al. 1998; Roberts & Weaver 2005).

Orientation of the AARM fabrics

Recently, the tectonic origin of magnetic fabrics of some CCPB sandstones was inferred from the results of in-phase and out-of-phase AMS and AARM measurements (Hrouda et al. 2018), suggesting that, in this case, the ferrimagnetic minerals are more sensitive recorders of a tectonic overprint than paramagnetic phyllosilicates. Consequently, the ferrimagnetic fabric should correspond to the compressional Early to Middle Miocene paleostress field documented by structural studies (Pešková et al. 2009; Vojtko et al. 2010; Sůkalová et al. 2012; Králiková et al. 2014).

The observed phyllosilicate–pyrite–ferrimagnetic iron oxide/sulphide association (Figs. 6, 7) and non-coaxiality between the AMS and AARM sub-fabrics indicate a complex relationship between strain, original sedimentary petrofabric (facies types), lithology and rheological contrast between para- and ferrimagnetic minerals.

Pyrite crystals are isotropic and seem to be resistant to tectonic deformation (Calvín et al. 2018a,b). As new ferrimagnetic minerals grow on the surface or inside the pyrite grains, they are influenced only by the stress conditions during their growth (Calvín et al. 2018a,b). On the other hand, during burial clay diagenesis, newly formed authigenic ferrimagnetic grains may grow mimetically with the preferred orientation of the parent clay minerals (Calvín et al. 2018a,b). Additionally, phyllosilicate minerals bearing the well-developed sedimentary/compaction AMS fabrics are resistant to further weak deformation (Parés & van der Pluijm 2002; Chadima et al. 2006; Pueyo Anchuela et al. 2011).

In the AARM type 1 the magnetic foliation strikingly coincides with the orientation of the joints while the Amax are distributed along the joints (sites 21, 17, Fig. 12). It may suggest a possibility of an inverse fabric (Rochette et al. 1992;

Ferré 2002) due to the expected presence of uniaxial single-domain authigenic magnetites (Potter & Stephenson 1988). The normal magnetic fabric with respect to the joints may result from the inverse orientation of single-domain magnetite grains to the joints (i.e. longer grain axes oriented perpendicular to the joints) with the Amax parallel to their short axis and Amin parallel to their longer axis (e.g. Chadima et al. 2009). Therefore, the single-domain magnetites could grow under fluid pressure during the opening of the joints (Hurai et al. 2002). The single-domain magnetites seemingly do not contribute to the bulk AMS fabric, which reflects the sedimentary petrofabric (sites 17, 21, Figs. 11, 12).

At site 21 the ferrimagnetic fabric is oriented differently in sandstones (AARM type 1) and mudstones (AARM type 2a) (Fig. 12). The difference can be a result of different response to deformation in sandstones and mudstones (Chadima et al. 2006). Mudstones contain more phyllosilicate minerals and show more flattened AMS fabric due to compaction (Fig. 8). The orientation of ferrimagnetic minerals partly mimic the original AMS fabric, because the magnetic foliation remained parallel to the bedding while the Amax is oriented to the N–S direction, slightly deflected from the joint to bedding intersection (Fig. 12). The deflection of the Amax could be apparent because the joints are less developed and more scattered in the mudstones than in the more competent sandstones (Ludwiniak 2010). For example, the Amax parallel to the bedding /joint intersection is more clearly visible in the massive and parallel-laminated sandstones at site 2 (AARM type 2b, Fig. 12). The N-NW oriented Amax were also observed in mudstones from several localities in the Podhale Basin (Márton et al. 2009a). The AARM type 2 most probably reflects the compressive regime in which the joints started to develop (Ludwiniak 2010; 2018; Ludwiniak et al. 2019).

The coincidence between the AARM and AMS fabric (AARM type 3) was observed in the convoluted sandstones at site 30 (Fig. 12). Paramagnetic phyllosilicates, the source of the AMS fabric, were re-oriented early after deposition by processes generating convolutions, followed by pyrite formation (Fig. 6H), and eventually by pyrite alteration due to burial and neoformation of ferrimagnetic minerals. In this case, the deformation was not strong enough to affect ferrrimagnetic minerals, so they mimic the original syn-sedimentary to early diagenetic AMS fabric. Alternatively, burial clay transformation processes (e.g. Katz et al. 1998) could be more dominant in this part of the basin and the ferrimagnetic minerals grew mimetically with the parent phyllosilicates (Fig. 6H).

The distinct ferrimagnetic populations were indicated in an experiment where we re-measured the AARM type 1 after heating samples to 580 °C (samples SMP466A, SMP478A, site 17 in Fig. 12). After the heating, the original AARM fabric was destroyed and the heating produced a new ferrimagnetic mineral, which mimics the sedimentary AMS fabric. It implies that the paramagnetic phyllosilicates and ferrimagnetic phases were not originally related and the pyrite oxidation seems to be the more dominant process in neoformation of ferrimagnetic minerals in turbidite deposits of the CCPB.

Conclusions

This study revealed that in the Oligocene turbidites of the CCPB, the AMS fabrics are dominantly of sedimentary origin. They are governed mostly by the preferred orientation of paramagnetic phyllosilicate minerals. The Kmax in the Ta–Tb–Tc turbidite intervals are well-clustered and oriented parallel to the measured paleoflow directions. The well-grouped Kmax in the mudstone facies (Te interval) coincide with the local paleoflow directions measured on the intercalated turbidite sandstones or directly on the mudstones, suggesting that the mudstones were deposited during the final stages of waning dilute turbidite flows. The AMS fabric in the hydroplastically deformed facies such as convolute and slump folded sandstones reflects the soft-sediment deformation structures.

The comparison of the AMS fabrics, especially, between organized Ta–Te turbidite intervals and the hydroplastically deformed facies proved to be an effective way of distinguishing an original sedimentary from a tectonically induced magnetic fabric in weakly deformed turbidite deposits. As the turbidite deposits were affected by compression, in the Miocene, the sedimentary origin of the AMS fabrics was further supported by the poor correlation between the bedding strikes and AMS lineations.

The implication of our study is that once the sedimentary origin of magnetic fabric in turbidite deposits is proved, the AMS lineations from any of the Ta–Te intervals seem to give useful information about paleoflow orientations.

The AARM and the AMS fabrics are oriented differently. The former seem to be genetically related to the formation of the diagonal conjugate joint set. We could distinguish three types of the AARM fabrics. The AARM type 1 represents magnetic foliations oriented parallel to the joints while magnetic lineations are distributed along the joints. The AARM type 2 shows signs of transitional sedimentary to tectonic magnetic fabric and the AARM type 3 coincides with the sedimentary AMS fabric.

Magnetic mineralogy experiments documented dominant magnetite accompanied by ferrimagnetic iron sulphides. Both seem to be authigenic phases associated with pyrite, as the microscopic investigations (SEM, WDS) revealed. These sub-microscopic phases formed during late diagenesis through the alteration of pyrite, possibly accompanied by clay transformation processes during burial. The growth of the authigenic ferrimagnetic minerals was conditioned by combined effects of the sedimentary petrofabric, lithology and stress conditions during the inversion of the basin in the Early to Middle Miocene.

Acknowledgements: The study was financially supported by the National Development and Innovation Office of Hungary (project K128625), the Slovak Research and Development Agency (former project APVV-0212-12 and running project APVV-17-0170) and by the VEGA Agency (projects 2/0028/17, 2/0014/18 and 2/0013/20). We thank Tünde Cséfán, Gábor Imre, Juraj Šurka and several members of my

family (JM) for their technical assistance in the field and laboratory. Thanks to Sergii Kurylo for his help with the SEM analysis. We thank Pablo Calvín, František Hrouda and Anna Wysocka for their detailed and valuable reviews that helped to improve the first draft. Editorial handling by Ján Soták is appreciated.

References

Allen J.R.L. 1982: Sedimentary structures: their character and physical basis Volume 2. *Developments in Sedimentology* 30B, *Elsevier*, Amsterdam, 1–663.

Almqvist B.S.G. & Koyi H. 2018: Bulk strain in orogenic wedges based on insights from magnetic fabrics in sandbox models. *Geology* 46, 483–486. https://doi.org/10.1130/G39998.1

Aubourg Ch. & Pozzi J-P. 2010: Toward a new <250 ºC pyrrhotite–magnetite geothermometer for claystones. *Earth Planetary Science Letters* 294, 47–57. https://doi.org/10.1016/j.epsl.2010.02.045

Aubourg Ch., Pozzi J-P. & Kars M. 2012: Burial, claystones remagnetization and some consequences for magnetistratigraphy. In: Elmore R.D., Muxworthy A.R., Aldana M.M. & Mena M. (Eds.): Remagnetization and chemical alteration of sedimentary rocks. *Geological Society, London, Special Publications* 371, 181–188. https://doi.org/10.1144/SP371.4

Averbuch O., Frizon de Lamotte D. & Kissel C. 1992: Magnetic fabric as a structural indicator of the deformation path within a fold-thrust structure: a test case from the Corbières (NE Pyrenees, France). *Journal of Structural Geology* 14, 461–474. https://doi.org/10.1016/0191-8141(92)90106-7

Baas J.H., Hailwood E.A., McCaffrey W.D., Kayc M. & Jones R. 2007: Directional petrological characterisation of deep-marine sandstones using grain fabric and permeability anisotropy: methodologies, theory, application and suggestions for integration. *Earth-Science Reviews* 82, 101–142. https://doi.org/10.1016/j.earscirev.2007.02.003

Banerjee S., Elmore D.R. & Engel M.H. 1997: Chemical remagnetization and burial diagenesis: Testing the hypothesis in Pennsylvanian Belden Formation, Colorado. *Journal of Geophysical Research* 102, 24825–24842. https://doi.org/10.1029/97JB01893

Bezák V., Broska I., Ivanička J., Reichwalder P., Vozár J., Polák M., Havrila M., Mello J., Biely A., Plašienka D., Potfaj M., Konečný V., Lexa J., Kaličiak M., Žec B., Vass D., Elečko M., Janočko J., Pereszlényi M., Marko F., Maglay J. & Pristaš J. 2004: Tectonic map of Slovak Republic. *Ministry of Environment*, *State Geological Institute of Dionýz Štúr*, Bratislava.

Borradaile G.J. & Jackson M. 2010: Structural geology, petrofabrics and magnetic fabrics (AMS, AARM, AIRM). *Journal of Structural Geology* 32, 1519–1551. https://doi.org/10.1016/j.jsg.2009.09.006

Bouma A.H. 1962: Sedimentology of some flysch deposits. *Elsevier*, Amsterdam, 1–168.

Calvín P., Villalaín J.J. & Casas-Sainz A.M. 2018a: The carriers of AMS in remagnetized carbonates. Insights for remagnetization mechanism and basin evolution. *Physics of the Earth and Planetary Interiors* 282, 1–20. https://doi.org/10.1016/j.pepi.2018.06.003

Calvín P., Villalaín J.J. & Casas-Sainz A.M. 2018b: Anisotropic magnetite growth in remagnetized limestones: Tectonic constrains and implications for basin history. *Geology* 46, 751–754. https://doi.org/10.1130/G45158.1

Chadima M. & Jelínek V. 2008: Anisoft 4.2. – Anisotropy data browser. In: Paleo, Rock and Environmental Magnetism: 11th Castle Meeting, 22–28 June 2008, Bojnice. *Contribution to Geophysics and Geodesy* 38, 41.

Chadima M., Hrouda F. & Melichar R. 2006: Magnetic fabric study of the SE Rhenohercynian Zone (Bohemian Massif): Implications for dynamics of the Paleozoic accretionary wedge. *Tectonophysics* 418, 93–109. https://doi.org/10.1016/j.tecto.2005.12.015

Chadima M., Cajz V. & Týcová P. 2009: On the interpretation of normal and inverse magnetic fabric in dikes: Examples from the Eger Graben, NW Bohemian Massif. *Tectonophysics* 466, 47–63. https://doi.org/10.1016/j.tecto.2008.09.005

Cifelli F., Mattei M., Chadima M., Hirt A.M. & Hansen A. 2005: The origin of tectonic lineation in extensional basins: combined neutron texture and magnetic analyses on "undeformed" clays. *Earth Planetary Science Letters* 235, 62–78. https://doi.org/10.1016/j.epsl.2005.02.042

Cifelli F., Mattei M., Chadima M., Lenser S. & Hirt A.M. 2009: The magnetic fabric in "undeformed clays": AMS and neutron texture analyses from the Rif Chain (Morocco), *Tectonophysics* 466, 79–88. https://doi.org/10.1016/j.tecto.2008.08.008

Dall'Olio E., Felletti F. & Muttoni G. 2013: Magnetic-fabric analysis as a tool to constrain mechanisms of deep-water mudstone deposition in the Marnoso Arenacea Formation (Miocene, Italy). *Journal of Sedimentary Research* 83, 170–182. https://doi.org/10.2110/jsr.2013.12

Elmore R.D., Muxworthy A.R. & Aldana M.M. 2012: Remagnetization and chemical alteration of sedimentary rocks. In: Elmore R.D., Muxworthy A.R. Aldana, M.M. & Mena M. (Eds.): Remagnetization and chemical alteration of sedimentary rocks. *Geological Society, London, Special Publications* 371, 1–21. https://doi.org/10.1144/SP371.15

Ferré E.C. 2002: Theoretical models of intermediate and inverse AMS fabrics. *Geophysical Research Letters* 29, 1127. https://doi.org/10.1029/2001GL014367

Felletti F., Dall'Olio E. & Muttoni G. 2016: Determining flow directions in turbidites: An integrated sedimentological and magnetic fabric study of the Miocene Marnoso Arenacea Formation (northern Apennines, Italy). *Sedimentary Geology* 335, 197–215. https://doi.org/10.1016/j.sedgeo.2016.02.009

Filo I. & Siráňová Z. 1996: The Tomášovce Member – A new lithostratigraphic Unit of the Subtatric Group. *Geologické Práce, Správy* 102, 41–49 (in Slovak with English summary).

Filo I. & Siráňová Z. 1998: Hornád and Chrasť Members – new regional lithostratigraphic units of the Sub-tatric Group. *Geologické Práce, Správy* 103, 35–51 (in Slovak with English summary).

García-Lasanta C., Oliva-Urcia B., Román-Berdiel T., Casas A.M. & Pérez-Lorente F. 2013: Development of magnetic fabric in sedimentary rocks: insights from early compactional structures. *Geophysical Journal International* 194, 182–199. https://doi.org/10.1093/gji/ggt098

Garecka M. 2005: Calcareous nannoplankton from the Podhale Flysch (Oligocene–Miocene, Inner Carpathians, Poland). In: Tyszka J., Oliwkiewicz-Miklasińska M., Gedl P. & Kaminski M.A. (Eds.): Methods and applications in micropalaeontology. *Studia Geologica Polonica* 124, 353–369.

Gedl P. 2000: Palaeogeography of the Podhale Flysch (Oligocene; Central Carpathians, Poland) – its relation to the neighbourhood areas as based on palynological studies. *Slovak Geological Magazine* 2–3, 150–154.

Gołab J. 1959: On the geology of the western Podhale Flysch area. *Instytut Geologiczny, Biuletyn* 149, 225–237.

Gregorová D., Hrouda F. & Kohút M. 2009: Magnetic fabric of granitic composite pluton of the Veľká Fatra Mountains (Western Carpathians, Slovakia): A Variscan remnant within the Alpine edifice? *Geodinamica Acta* 22, 57–72. https://doi.org/10.3166/ga.22.57-72

Gross P. 1998: Kežmarok Beds – A new lithostratigraphic unit of the Sub-tatric Group *Geologické Práce, Správy* 103, 27–33 (in Slovak).

Gross P. 2008: Lithostratigraphy of Western Carpathians: Paleogene – Podtatranská Group. *State Geological Institute of Dionýz Štúr*, Bratislava, 1–78 (in Slovak with English summary).

Gross P., Köhler E. & Borza K. 1982: Conglomerate submarine fans in Central-Carpathian Paleogene near Pucov. *Geologické Práce, Správy* 77, 75–86 (in Slovak with English summary).

Gross P., Köhler E. & Samuel O. 1984: A new lithostratigraphical division of the Inner-Carpathian Paleogene. *Geologické Práce, Správy* 81, 113–117 (in Slovak with English summary).

Hrouda F. 1982: Magnetic anisotropy of rocks and its application in geology and geophysics. *Geophysical Surveys* 5, 37–82. https://doi.org/10.1007/BF01450244

Hrouda F. & Potfaj M. 1993: Deformations of sediments in the post-orogenic Intra-Carpathian Paleogene Basin as indicated by magnetic anisotropy. *Tectonophysics* 224, 425–434. https://doi.org/10.1016/0040-1951(93)90042-I

Hrouda F., Jelínek V. & Hrušková L. 1990: A package of programs for statistical evaluation of magnetic anisotropy data using IBM PC computers. *EOS, Transactions, American Geophysical Union, Fall meeting 1990*, 1289.

Hrouda F., Krejčí O., Potfaj M. & Stráník Z. 2009: Magnetic fabric and weak deformation in sandstones of accretionary prisms of the Flysch and Klippen Belts of the Western Carpathians: Mostly offscraping indicated. *Tectonophysic*s 479, 254–270. https://doi.org/10.1016/j.tecto.2009.08.016

Hrouda F., Gilder S., Wack M. & Ježek J. 2018: Diverse response of paramagnetic and ferromagnetic minerals to deformation from Intra-Carpathian Paleogene sedimentary rocks: Comparison of magnetic susceptibility and magnetic remanence anisotropies. *Journal of Structural Geology* 113, 217–224. https://doi.org/10.1016/j.jsg.2018.06.001

Hurai V., Širaňová V., Marko F. & Soták J. 1995: Hydrocarbons in fluid inclusions from quartz–calcite veins hosted in Paleogene flysch sediments of the Central Carpathians. *Mineralia Slovaca* 27, 383–396 (in Slovak with English summary).

Hurai V., Kihle J., Kotulová J., Marko F. & Świerczewska A. 2002: Origin of methane in quartz crystals from the Tertiary accretionary wedge and fore-arc basin of the Western Carpathians. *Applied Geochemistry* 17, 1259–1271. https://doi.org/10.1016/S0883-2927(01)00128-7

Hurai V., Tokarski A.K., Świerczewska A., Kotulová J., Biroň A., Soták J., Hrušecký I. & Marko F. 2004: Methane degassing and exhumation of the Tertiary accretionary complex and fore-arc basin of the Western Carpathians. *Geolines* 17, 42–45.

Hurai V., Marko F., Tokarski A.K., Świerczewska A., Kotulová J. & Biroň A. 2006: Fluid inclusion evidence for deep burial of the Tertiary accretionary wedge of the Carpathians. *Terra Nova* 18, 440–446. https://doi.org/10.1111/j.1365-3121.2006.00710.x

Janočko J. 2002: Central-Carpathian Paleogene basin – evolution and depositional systems. *Mineralia Slovaca* 34, 159–180 (in Slovak with English summary).

Janočko J. & Jacko S. 1998: Marginal and deep-sea deposits of Central-Carpathian Paleogene Basin, Spišská Magura region, Slovakia: Implication for basin history. *Slovak Geological Magazine* 4, 281–292.

Janočko J., Hamršmíd B., Jacko S. & Siráňová Z. 1998: Suprafan and chanell-and-levee deposits near Tichý Potok, Levoča Mts.; Central-Carpathian Paleogene Basin, Slovakia. *Slovak Geological Magazine* 4, 3–15.

Janočko J., Gross P., Polák M., Potfaj M., Jacko S. jr., Rakús M., Halouzka R., Jetel J., Petro Ľ., Kubeš P., Buček S., Köhler E., Siráňová Z., Zlínska A., Halasová E., Hamršmíd B., Karoli S., Žec B., Fejdiová O., Milička J., Boorová D. & Žecová K. 2000: Explanations to geological map of the Spišská Magura Mts., 1:50 000. *State Geological Institute of Dionýz Štúr*, Bratislava, 1–202 (in Slovak with English summary).

Jelínek V. 1977: The statistical theory of measuring anisotropy of magnetic susceptibility of rocks and its applications. *Geofyzika n.p.*, Brno, 1–88.

Jelínek V. 1978: Statistical processing of magnetic susceptibility measured on groups of specimens. *Studia Geophysica et Geodaetica* 22, 50–62.

Jelínek V. 1981: Characterization of magnetic fabric of rocks. *Tectonophysics* 79, T61–T67. https://doi.org/10.1016/0040-1951(81)90110-4

Jelínek V. 1993: Theory and measurement of the anisotropy of isothermal remanent magnetization of rocks. *Travaux Géophysiques* 37, 124–134.

Jiang W-T., Horng CH-S., Roberts A.P. & Peacor D.R. 2001: Contradictory magnetic polarities in sediments and variable timing of neoformation of authigenic greigite. *Earth Planetary Science Letters* 193, 1–12. https://doi.org/10.1016/S0012-821X(01)00497-6

Kars M., Aubourg Ch., Labaume P., Berquó T.S. & Cavailhes T. 2014: Burial diagenesis of magnetic minerals: new insights from the Grès d´Annot Transect (SE France). *Minerals* 4, 667–689. https://doi.org/10.3390/min4030667

Katz B., Elmore R.D. & Cogoini M. 1998: Widespread chemical remagnetization: Orogenic fluids or burial diagenesis of clays? *Geology* 26, 603–606. https://doi.org/10.1130/0091-7613(1998)026%3C0603:WCROFO%3E2.3.CO;2

Kázmér M., Dunkl I., Frisch W., Kuhlemann J. & Ozsvárt P. 2003: The Paleogene forearc basin of the Eastern Alps and Western Carpathians: subduction erosion and basin evolution. *Journal of the Geological Society* 160, 413–428. https://doi.org/10.1144/0016-764902-041

Kissel C., Barrier E., Laj C. & Lee T. 1986: Magnetic fabric in 'undeformed' marine clays from compressional zones. *Tectonics* 5, 769–781. https://doi.org/10.1029/TC005i005p00769

Kneller B. & Branney M.J. 1995: Sustained high-density turbidity currents and the deposition of thick massive sands. *Sedimentology* 42, 607–616. https://doi.org/10.1111/j.1365-3091.1995.tb00395.x

Kodama K.P. 2012: Paleomagnetism of sedimentary rocks. Process and interpretation. *Wiley-Blackwell*, Chichester, 1–157.

Kováč M., Plašienka D., Soták J., Vojtko R., Oszczypko N., Less G., Ćosović V., Fügenschuh B. & Králiková S. 2016: Paleogene palaeogeography and basin evolution of the Western Carpathians, Northern Pannonian domain and adjoining areas. *Global Planetary Change* 140, 9–27. https://doi.org/10.1016/j.gloplacha.2016.03.007

Kováč P. & Hók J. 1996: Tertiary development of the western part of Klippen Belt. *Slovak Geological Magazine* 2, 136–149.

Králiková S., Vojtko R., Sliva Ľ., Minár J., Fügenschuh B., Kováč M. & Hók J. 2014: Cretaceous–Quaternary tectonic evolution of the Tatra Mts (Western Carpathians): constraints from structural, sedimentary, geomorphological, and fission track data. *Geologica Carpathica* 65, 307–326. https://doi.org/10.2478/geoca-2014-0021

Larrasoaña J.C., Pueyo E.L. & Parés J.M. 2004: An integrated AMS, structural, palaeo and rock-magnetic study of Eocene marine marls from the Jaca-Pamplona Basin (Pyrenees, N Spain); new insights into the timing of magnetic fabric acquisition in weakly deformed mudrocks. In: Martín-Hernández F., Lüneburg C.M., Aubourg C. & Jackson M. (Eds.): Magnetic Fabrics: methods and applications. *Geological Society, London, Special Publications* 238, 127–143. https://doi.org/10.1144/GSL.SP.2004.238.01.10

Lowe D.R. 1975: Water escape structures in coarse grained sediments. *Sedimentology* 22, 157–204. https://doi.org/10.1111/j.1365-3091.1975.tb00290.x

Lowrie W. 1990: Identification of ferromagnetic minerals in a rock by coercivity and unblocking temperature properties. *Geophysical Research Letters* 17, 159–162. https://doi.org/10.1029/GL017i002p00159

Ludwiniak M. 2010: Multi-stage development of the joint network in the flysch rocks of western Podhale (Inner Western Carpathians, Poland). *Acta Geologica Polonica* 60, 283–316.

Ludwiniak M. 2018: Miocene transpression effects at the boundary of Central Carpathian Paleogene Basin and Pieniny Klippen Belt: examples from Polish – Slovakian borderland. *Geology Geophysics and Environment* 44, 91–110. https://doi.org/10.7494/geol.2018.44.1.91

Ludwiniak M. Śmigielski M., Kowalczyk S., Łoziński M., Czarniecka U. & Lewińska L. 2019: The intramontane Orava Basin – evidence of large-scale Miocene to Quaternary sinistral wrenching in the Alpine–Carpathian–Pannonian area. *Acta Geologica Polonica* 69, 339–386.

Marschalko R. 1966: Origin and depositional history of Basal Formation (Central Carpathian Paleogene). *Geologický Sborník* 17, 311–335.

Marschalko R. 1968: Facies distribution, paleocurrents and paleotectonics of the Paleogene flysch of Central West Carpathians. *Geologický Zborník – Geologica Carpathica* 19, 69–94.

Marschalko R. 1970: The research of sedimentary textures, structures, and palaeocurrent analysis of basal formations (Central Western Carpathian Paleogene, N of Spišsko-gemerské rudohorie Mts.). *Acta Geologica et Geographica Universitatis Comenianae* 19, 129–163.

Marschalko R. & Gross P. 1970: Deep submarine erosion in turbidite sequences, Central-Carpathian Flysch, Levočské Pohorie Mts. *Geologický Zborník – Geologica Carpathica* 21, 167–174.

Marschalko R. & Radomski A. 1960: Preliminary results of investigations of current directions in the flysch basin of the Central Carpathians. *Annales Societatis Geologurum Poloniae* 30, 259–272.

Mattei M., Sagnotti L., Faccenna C. & Funiciello R. 1997: Magnetic fabric of weakly deformed clay-rich sediments in the Italian peninsula: Relationships with compressional and extensional tectonics. *Tectonophysics* 271, 107–122. https://doi.org/10.1016/S0040-1951(96)00244-2

Mattei M., Speranza F., Argentieri A., Rosseti F., Sagnotti L. & Funiciello R. 1999: Extensional tectonics in the Amantea basin (Calabria, Italy): a comparison between structural and magnetic anisotropy data. *Tectonophysics* 307, 33–49. https://doi.org/10.1016/S0040-1951(99)00117-1

Márton E. 2020: Last scene in the large scale rotations of the Western Carpathians as reflected in paleomagnetic constraints. *Geology Geophysics and Environment* 46, 109–133. https://doi.org/10.7494/geol.2020.46.2.109

Márton E. & Fodor L. 1995: Combination of palaeomagnetic and stress data – a case study from North Hungary. *Tectonophysics* 242, 99–114. https://doi.org/10.1016/0040-1951(94)00153-Z

Márton E. & Fodor L. 2003: Tertiary paleomagnetic results and structural analysis from the Transdanubian Range (Hungary): rotational disintegration of the Alcapa unit. *Tectonophysics* 363, 201–224. https://doi.org/10.1016/S0040-1951(02)00672-8

Márton E., Mastella L. & Tokarski K.A. 1999: Large counter-clockwise rotation of the Inner West Carpathian Paleogene Flysch – Evidence from paleomagnetic investigations of the Podhale Flysch (Poland). *Physics and Chemistry of the Earth, Part A: Solid Earth and Geodesy* 24, 645–649. https://doi.org/10.1016/S1464-1895(99)00094-0

Márton E., Jeleńska M., Tokarski K.A., Soták J., Kováč M. & Spišiak J. 2009a: Current independent paleomagnetic declinations in flysch basins: a case study from the Inner Carpathians. *Geodinamica Acta* 22, 73–82. https://doi.org/10.3166/ga.22.73-82

Márton E., Rauch-Włodarska M., Krejči O., Tokarski A.K. & Bubik M. 2009b: An integrated palaeomagnetic and AMS study of the Tertiary flysch from the Outer Western Carpathians. *Geophysical Journal International* 177, 925–940. https://doi.org/10.1111/j.1365-246X.2009.04104.x

Márton E., Tomljenović B., Pavelić D., Pethe M. & Jelen B. 2012: Magnetic fabric of Late Miocene clay-rich sediments from the southern Pannonian basin. *International Journal of Earth Sciences* 101, 879–888. https://doi.org/10.1007/s00531-011-0669-8

Márton E., Grabowski J., Plašienka D., Túnyi I., Krobicki M., Haas J. & Pethe M. 2013: New paleomagnetic results from the Upper Cretaceous red marls of the Pieniny Klippen Belt, Western Carpathians: evidence for general CCW rotation and implications for the origin of the structural arc formation. *Tectonophysics* 592, 1–13. https://doi.org/10.1016/j.tecto.2013.01.027

Márton E., Grabowski J., Tokarski A.K. & Túnyi I. 2016: Palaeomagnetic results from the fold and thrust belt of the Western Carpathians: an overview. In: Pueyo E.L., Cifelli F., Sussman A.J. & Oliva-Urcia B. (Eds.): Palaeomagnetism in fold and thrust belts: new perspectives. *Geological Society, London, Special Publications* 425, 7–36. https://doi.org/10.1144/SP425.1

Mills P.C. 1983: Genesis and diagnostic value of soft-sediment deformation structures – a review. *Sedimentary Geology* 35, 83–104. https://doi.org/10.1016/0037-0738(83)90046-5

Mutti E. 1992: Turbidite sandstones. *AGIP, Istituto di Geologia, Universita`di Parma*, 1–275.

Neuwerth R., Suter F., Guzman C.A. & Gorin G.E. 2006: Soft-sediment deformation in a tectonically active area: The Plio-Pleistocene Zarzal Formation in the Cauca Valley (Western Colombia). *Sedimentary Geology* 186, 67–88. https://doi.org/10.1016/j.sedgeo.2005.10.009

Olszewska B.W. & Wieczorek J. 1998: The Paleogene of the Podhale Basin (Polish Inner Carpathians) – micropaleontological perspective. *Przegląd Geologiczny* 46, 721–728.

Owen G. 1987: Deformation processes in unconsolidated sands. In: Jones M.E. & Preston R.M.F. (Eds.): Deformation of sediments and sedimentary rocks, *Geological Society, London, Special Publications* 29, 11–24. https://doi.org/10.1144/GSL.SP.1987.029.01.02

Owen G. 1996: Experimental soft-sediment deformation structures formed by the liquefaction of unconsolidated sands and some ancient examples. *Sedimentology* 43, 279–293. https://doi.org/10.1046/j.1365-3091.1996.d01-5.x

Parés J.M. 2015: Sixty years of anisotropy of magnetic susceptibility in deformed sedimentary rocks. *Frontiers in Earth Science* 3, 1–13. https://doi.org/10.3389/feart.2015.00004

Parés J.M. & van der Pluijm B.A. 2002: Evaluating magnetic lineations (AMS) in deformed rocks. *Tectonophysics* 350, 283–298. https://doi.org/10.1016/S0040-1951(02)00119-1

Parés J.M., van der Pluijm B.A. & Dinarès-Turell J. 1999: Evolution of magnetic fabrics during incipient deformation of mudrocks (Pyrenees, northern Spain). *Tectonophysics* 307, 1–14. https://doi.org/10.1016/S0040-1951(99)00115-8

Pešková I., Vojtko R., Starek D. & Sliva L. 2009: Late Eocene to Quarternary deformation and stress field evolution of the Orava region (Western Carpathians). *Acta Geologica Polonica* 59, 73–91.

Pickering K.T., Stow D.A.V., Watson M.P. & Hiscott R.N. 1986: Deep-water facies, processes and models: a review and classification scheme for modern and ancient sediments. *Earth-Science Reviews* 23, 75–174. https://doi.org/10.1016/0012-8252(86)90001-2

Piper D.J.W. 1978: Turbidite muds and silts on deep-sea fans and abyssal plains. In: Stanley D.J. & Kelling G. (Eds.): Sedimenta-

tion in submarine canyons, fans and trenches. *Dowden, Hutchinson and Ross*, Stroudsburg, 163–176.

Piper J.D.A., Elliot M.T. & Kneller B.C. 1996: Anisotropy of magnetic susceptibility in a Palaeozoic flysch basin: the Windermere Supergroup, northern England. *Sedimentary Geology* 106, 235–258. https://doi.org/10.1016/S0037-0738(96)00011-5

Plašienka D. 2018: Continuity and episodicity in the early Alpine tectonic evolution of the Western Carpathians: how large-scale processes are expressed by the orogenic architecture and rock record data. *Tectonics* 37, 2029–2079. https://doi.org/10.1029/2017TC004779

Plašienka D., Grecula P., Putiš M., Kováč M. & Hovorka D. 1997: Evolution and structure of the Western Carpathians: An overview. In: Grecula P., Hovorka D. & Putiš M. (Eds.): Geological evolution of the Western Carpathians: an overview. *Mineralia Slovaca–Monograph,* 1–24.

Plašienka D., Bučová J. & Šimonová V. 2019: Variable structural styles and tectonic evolution of an ancient backstop boundary: the Pieniny Klippen Belt of the Western Carpathians. *International Journal of Earth Sciences* 109, 1355–1376. https://doi.org/10.1007/s00531-019-01789-5

Potter D.K. & Stephenson A. 1988: Single-domain particles in rocks and magnetic fabric analysis. *Geophysical Research Letters* 15, 1097–1100. https://doi.org/10.1029/GL015i010p01097

Pueyo Anchuela Ó., Gil Imaz A., Pocoví Juan A. & Ipas Lloréns J.F. 2011: Acquisition and blocking of magnetic fabrics in synsedimentary structures, Eocene Pyrenees, Spain. *Geophysical Journal International* 186, 1015–1028. https://doi.org/10.1111/j.1365-246X.2011.05136.x

Ratschbacher L., Frisch W., Linzer H.-G., Sperner B., Meschede M., Decker K., Nemčok M., Nemčok J. & Grygar R. 1993: The Pieniny Klippen Belt in the Western Carpathians of northeastern Slovakia: structural evidence for transpression. *Tectonophysics* 226, 471–483. https://doi.org/10.1016/0040-1951(93)90133-5

Rees A.I. 1965: The use of anisotropy of magnetic susceptibility in the estimation of sedimentary fabric. *Sedimentology* 4, 257–271. https://doi.org/10.1111/j.1365-3091.1965.tb01550.x

Roberts A.P. & Weaver R. 2005: Multiple mechanisms of remagnetization involving sedimentary greigite (Fe_3S_4). *Earth Planetary Science Letters* 231, 263–277. https://doi.org/10.1016/j.epsl.2004.11.024

Rochette P. 1987: Magnetic susceptibility of the rock matrix related to magnetic fabric studies. *Journal of Structural Geology* 9, 1015–1020. https://doi.org/10.1016/0191-8141(87)90009-5

Rochette P., Jackson M. & Aubourgh C. 1992: Rock magnetism and interpretation of anisotropy of magnetic susceptibility. *Reviews of Geophysics* 30, 209–226. https://doi.org/10.1029/92RG00733

Roniewicz P. 1969: Sedimentation of the Nummulite Eocene in the Tatry Mts. *Acta Geologica Polonica* 19, 503–608 (in Polish).

Royden L.H. & Báldi T. 1988: Early Cenozoic tectonics and paleogeography of the Pannonian Basin and surrounding regions. In: Royden L.H. & Horváth F. (Eds.): The Pannonian Basin. A Study in Basin Evolution. *AAPG Memoir* 45, 1–16. https://doi.org/10.1306/M45474C1

Schwehr K. & Tauxe L. 2003: Characterization of soft-sediment deformation: Detection of cryptoslumps using magnetic methods. *Geology* 31, 203–206. https://doi.org/10.1130/0091-7613(2003)031%3C0203:COSSDD%3E2.0.CO;2

Soták J. 2010: Paleoenvironmental changes across the Eocene–Oligocene boundary: insights from the Central-Carpathian Paleogene Basin. *Geologica Carpathica* 61, 393–418. https://doi.org/10.2478/v10096-010-0024-1

Soták J., Pereszlenyi M., Marschalko R., Milička J. & Starek D. 2001: Sedimentology and hydrocarbon habitat of the submarine-fan deposits of the Central Carpathian Paleogene Basin (NE Slovakia). *Marine Petroleum Geology* 18, 87–114. https://doi.org/10.1016/S0264-8172(00)00047-7

Soták J., Gedl P., Banská M. & Starek D. 2007: New stratigraphic data from the Paleogene formations of the Central Western Carpathians in the Orava region: results of integrated micropaleontological study in the Pucov section. *Mineralia Slovaca* 39, 89–106.

Soto R., Larrasoaña J.C, Arlegui L.E., Beamud E., Oliva-Urcia B. & Simón J.L. 2009: Reliability of magnetic fabric of weakly deformed mudrocks as a palaeostress indicator in compressive settings. *Journal of Structural Geology* 31, 512–522. https://doi.org/10.1016/j.jsg.2009.03.006

Środoń J., Kotarba M., Biroň A., Such P., Clauer N. & Wójtowicz A. 2006: Diagenetic history of the Podhale-Orava Basin and the underlying Tatra sedimentary structural units (Western Carpathians): Evidence from XRD and K–Ar of illite–smectite. *Clay Minerals* 41, 751–774. https://doi.org/10.1180/0009855064130217

Stachowska A., Łoziński M., Śmigielski M., Wysocka A., Jankowski L. & Ziółkowski P. 2020: Anisotropy of magnetic susceptibility as an indicator for paleocurrent analysis in folded turbidites (Outer Western Carpathians, Poland). *Sedimentology* 67, 3783–3808. https://doi.org/10.1111/sed.12770

Starek D. & Fuksi T. 2017a: Distal turbidite fan/lobe succession of the Late Oligocene Zuberec Fm. – architecture and hierarchy (Central Western Carpathians, Orava-Podhale basin). *Open Geosciences* 9, 385–406. https://doi.org/10.1515/geo-2017-0030

Starek D. & Fuksi T. 2017b: Statistical analysis as a tool for identification of depositional palaeoenvironments in deep-sea fans (Palaeogene formations, Central Western Carpathians, north Slovakia). *Acta Geologica Slovaca* 9, 149–162.

Starek D., Andreyeva-Grigorovich A.S. & Soták J. 2000: Suprafan deposits of the Biely Potok Fm. in the Orava region: Sedimentary facies and nannoplankton distribution. *Slovak Geological Magazine* 2, 188–190.

Starek D., Sliva Ľ. & Vojtko R. 2004: The channel-levee sedimentary facies and their synsedimentary deformation: a case study from Huty Fm. of the Podtatranská skupina Group (Western Carpathians). *Slovak Geological Magazine* 10, 177–182.

Starek D., Sliva Ľ. & Vojtko R. 2012: Eustatic and tectonic control on late Eocene fan delta development (Orava Basin, Central Western Carpathians). *Geological Quarterly* 56, 67–84.

Starek D., Soták J., Jablonský J. & Marschalko R. 2013: Large-volume gravity flow deposits in the Central Carpathian Paleogene Basin (Orava region, Slovakia): evidence for hyperpycnal river discharge in deep-sea fans. *Geologica Carpathica* 64, 305–326. https://doi.org/10.2478/geoca-2013-0022

Starek D., Šimo V., Antolíková S. & Fuksi T. 2019: Turbidite sedimentology, biostratigraphy and paleoecology: A case study from the Oligocene Zuberec Fm. (Liptov Basin, Central Western Carpathians). *Geologica Carpathica* 70, 279–297. https://doi.org/10.2478/geoca-2019-0016

Suk D., Peacor D.R. & Van der Voo R. 1990: Replacement of pyrite framboids by magnetite in limestone and implications for paleomagnetism. *Nature* 345, 611–613.

Suk D., Van der Voo R. & Peacor D. R. 1993: Origin of magnetite responsible for remagnetization of Early Paleozoic limestones of New York State. *Journal of Geophysical Research* 98, 419–434. https://doi.org/10.1029/92JB01323

Sůkalová Ľ., Vojtko R. & Pešková I. 2012: Cenozoic deformation and stress field evolution of the Kozie chrbty Mountains and the western part of Hornad Depression (Central Western Carpathians). *Acta Geologica Slovaca* 4, 53–64.

Taira A. & Scholle P.A. 1979: Deposition of resedimented sandstone beds in the Pico Formation, Ventura Basin, California, as interpreted from magnetic fabric measurements. *Geological Society of America, Bulletin* 90, 952–962. https://doi.org/10.1130/0016-7606(1979)90%3C952:DORSBI%3E2.0.CO;2

Talling P.J., Masson D.G., Sumner E.J. & Malgesini J. 2012: Subaqueous sediment density flows: Depositional processes and deposit types. *Sedimentology* 59, 1937–2003. https://doi.org/10.1111/j.1365-3091.2012.01353.x

Tari G., Báldi T. & Báldi-Beke M. 1993: Paleogene retroarc flexural basin beneath the Neogene Pannonian Basin: a geodynamic model. *Tectonophysics* 226, 433–455. https://doi.org/10.1016/0040-1951(93)90131-3

Tarling D.H. & Hrouda F. 1993: The Magnetic Anisotropy of Rocks. *Chapman & Hall*, London, 1–217.

Tomek F., Žák J. & Chadima M. 2014: Magma flow paths and strain patterns in magma chambers growing by floor subsidence: a model based on magnetic fabric study of shallow-level plutons in the Štiavnica volcano–plutonic complex, Western Carpathians. *Bulletin of Volcanology* 76, 873. https://doi.org/10.1007/s00445-014-0873-z

Veloso E.E., Anma R., Ota T., Komiya T., Kagashima S. & Yamazaki T. 2007: Paleocurrent patterns of the sedimentary sequence of the Taitao ophiolite constrained by anisotropy of magnetic susceptibility and paleomagnetic analyses. *Sedimentary Geology* 201, 446–460. https://doi.org/10.1016/j.sedgeo.2007.07.005

Vojtko R., Tokárová E., Sliva Ľ. & Pešková I. 2010: Reconstruction of Cenozoic paleostress fields and revised tectonic history in the northern part of the Central Western Carpathians (the Spišská Magura and Východné Tatry Mountains). *Geologica Carpathica* 61, 211–225. https://doi.org/10.2478/v10096-010-0012-5

Vollmer F.W. 2015: Orient 3: a new integrated software program for orientation data analysis, kinematic analysis, spherical projections, and Schmidt plots. *Geological Society of America Abstracts with Programs* 47, 49.

Watycha L. 1959: Remarks on geology of the Podhale Flysch in the eastern part of Podhale. *Przegląd Geologiczny* 8, 350–356 (in Polish).

Westwalewicz-Mogilska E. 1986: A new look at the genesis of the Podhale Flysch. *Przegląd Geologiczny* 34, 690–698. (in Polish with English summary).

Whitney L.D. & Evans W.B. 2010: Abbreviations for names of rock-forming minerals. *American Mineralogist* 95, 185–187. https://doi.org/10.2138/am.2010.3371

Wieczorek J. 1989: The Hecho model for Podhale Flysch? *Przegląd Geologiczny* 37, 419–422 (in Polish).

Závada P., Calassou T., Schulmann K., Hrouda F., Štípská P., Hasalová P., Míková J., Magna T. & Mixa P. 2017: Magnetic fabric transposition in folded granite sills in Variscan orogenic wedge. *Journal of Structural Geology* 94, 166–183. https://doi.org/10.1016/j.jsg.2016.11.007

Supplementary Table 1 is available online at http://geologicacarpathica.com/data/files/supplements/GC-72-2-Madzin_Suppl_Table1.docx.